echnical Memorandum ERL AOML-37

# SURVEY OF SATELLITE SENSORS AND DATA WITH APPLICATION TO OTEC RESOURCE AND OPERATIONS REQUIREMENTS

George A. Maul
Fred M. Vukovich
Mark Bushnell
Bobby Crissman

Atlantic Oceanographic and Meteorological Laboratories
Miami, Florida
March 1979

noaa NATIONAL OCEANIC AND ATMOSPHERIC ADMINISTRATION / Environmental Research Laboratories

NOAA Technical Memorandum ERL AOML-37

# SURVEY OF SATELLITE SENSORS AND DATA WITH APPLICATION TO OTEC RESOURCE AND OPERATIONS REQUIREMENTS

George A. Maul
Fred M. Vukovich
Mark Bushnell
Bobby Crissman

Atlantic Oceanographic and Meteorological Laboratories
Miami, Florida
March 1979



UNITED STATES DEPARTMENT OF COMMERCE
Juanita M. Kreps, Secretary

NATIONAL OCEANIC AND ATMOSPHERIC ADMINISTRATION
Richard A. Frank, Administrator

Environmental Research Laboratories
Wilmot N. Hess, Director

NOTICE

The Environmental Research Laboratories do not approve, recommend, or endorse any proprietary product or proprietary material mentioned in this publication. No reference shall be made to the Environmental Research Laboratories or to this publication furnished by the Environmental Research Laboratories in any advertising or sales promotion which would indicate or imply that the Environmental Research Laboratories approve, recommend, or endorse any proprietary product or proprietary material mentioned herein, or which has as its purpose an intent to cause directly or indirectly the advertised product to be used or purchased because of this Environmental Research Laboratories publication.

TABLE OF CONTENTS

LIST OF FIGURES

LIST OF TABLES

# EXECUTIVE SUMMARY

Operational and experimental spacecraft are routinely observing ocean surface phenomena of importance to OTEC plant operations and site selection. This report summarizes the existing instruments and the capability of those instruments for observing geophysical variables that contribute to surface thermal resource fluctuations, the operating environment, and the impact of an OTEC plant on the ocean. The report consists of an introduction, a survey of satellites and satellite instruments of benefit to OTEC, examples of satellite data and potential OTEC uses, a summary (Table 10) of satellite sensors and data characteristics with reference to OTEC studies, a short glossary of acronyms, and an extensive list of references from a literature search.

The SEASAT-A experimental ocean-observing spacecraft ceased functioning after about 100 days due to an electrical failure in the power supply. A thorough discussion of the instruments is retained in this report because in the long term, similar instruments will probably be flown in operational vehicles (by mid-1980's). The NIMBUS-7 experimental spacecraft is functioning as designed at this writing, as is the GEOS-3 geodetic spacecraft, although it is three years old. Operational spacecraft such as TIROS-N, NOAA-4 and 5, and GOES-1, 2, 3 provide an important opportunity for long term monitoring and study of the historical data sets. No single spacecraft or sensor system provides all the useful observations for an OTEC concept; similarly, no satellite or instrument array provides observations that do not require in situ verification. Verification in the initial stages will involve surface ships, but future surface verification may be accomplished with unmanned platforms which transmit their data through one of the several existing satellite data collection systems.

For convenience to the reader, a summary table of satellite sensors and data characteristics is in chapter 4. Caution should be exercised in drawing conclusions that satellite observations as summarized in the table can solve all of the OTEC user's needs; they cannot. Satellite observations must be considered as part of an integrated observing and/or monitoring program within the overall OTEC data requirement.

At this writing, it is conjectural to list recommendations relating satellite sensors and data products to OTEC needs. Research is currently addressing the role satellite and in situ measurements should play in providing ocean thermal resource information. Geographically, OTEC plants are essentially confined to tropical ($\pm 30^{o}$) latitudes; this suggests that a geostationary spacecraft would provide proper coverage, and with current technology, can provide adequate temporal and spatial resolution for OTEC.

Preliminary result of assessing the presently operational geosynchronous vehicles (SMS and GOES), is that they are not capable of fully meeting the needs of the variety of OTEC plants being discussed. Optical sensors (visible and infrared) could be designed to provide the needed wavelength channels, calibration sources, and environmentally matched

resolutions for ocean thermal energy applications. Theoretically, microwave devices (which have all weather capability) could provide surface temperature and wind speed information, but as a practical matter, spatial resolution from a geostationary orbit would be too coarse due to antenna sizes. Polar orbiting spacecraft on the other hand, use their relative motion and position with respect to the sun and earth in order to obtain data not possible with a geostationary spacecraft. The trade-off usually is one of time dependence versus spatial resolution and/or observational technique. For OTEC thermal resource needs, however, high resolution (~ 3 km) information which can be interpreted in terms of plant intake temperatures is the highest operational priority. Equally important is the ability to assess the impact of a plant on the environment, and as in the case of thermal resource assessment, continued research is required in order to recommend an optimal observation system.

# 1.0 INTRODUCTION

Ocean Thermal Energy Conversion (OTEC) plants rely on ocean temperature differences between the upper layer (50 m or so) and some deep layer for their potential energy conversion. The oceanic upper layer is highly variable on scales from seconds, in the case of waves, to years, in the case of interannual heat storage changes. Observations of the variability in the upper layer can be extended in space and time by the application of remote sensing technology. The concept of measurement by remote sensing and the variables measurable are quite different from *in situ* observations, and it must be stated at the outset that any one technique (*in situ* or remote sensing) cannot satisfy all the OTEC user's needs.

Measurement of temperature exemplifies the differences between remote sensing and *in situ* observations. The infrared radiation leaving the sea is from a thin surface layer 10-20 μm thick and behaves according to Planck's Law. The sea surface is not a blackbody however: radiation is reflected according to the Fresnel equations, has an emissivity according to Kirchoff's Law, and due to evaporation, has a skin temperature that is different from the *in situ* temperature a few centimeters deeper in the fluid. The radiation measurement is an optical measurement and therefore covers a finite area of the sea surface. At satellite altitudes, this area is typically 1 km in diameter for a very high resolution radiometer and 10 km in diameter for a high resolution radiometer. The average radiation emitted by such an area is sensed at the satellite after the energy has passed through the atmosphere. Some of the infrared energy that is detected is absorbed by water vapor in the 10.5-12.5 μm region and re-emitted again at the temperature of the water vapor; scattering at infrared wavelengths is negligible as is quantified by Rayleigh's Law. Finally the received radiation is measured by photo detector devices which are calibrated by radiometric means, and is telemetered to ground receivers where the data are digitized and stored on magnetic tape. The noise equivalent temperature differences for the data handling equipment is of the order of 0.5°K.

From the summary given in the above paragraph, it should be clear that a comparison between *in situ* and remotely sensed temperatures is a non-trivial task. Remote sensing techniques depend on the measurement of electromagnetic radiation, and from that measurement, a physical variable such as temperature is inferred. The same physical principles govern the remote sensing of a number of other variables of value to OTEC research, development and operations: sea surface temperature, sea surface wind stress, near surface chlorophyll and phaeo-pigments, near surface suspended sediments, and near surface currents. No theoretically based methods of comparing remote sensing and *in situ* data have been developed, and accuracy statements are based on empirical correlations.

Chapter two of this report is a survey of the current U.S. spacecraft that have oceanographic measuring capability of value to the OTEC project. The instruments aboard each vehicle which provide useful measurements are described in some detail along with their design specification

accuracies and/or actual performance accuracies. Oceanographic interpretation of remote sensing data is in its infancy, and some new instruments (notably aboard SEASAT-A and NIMBUS-7) are virtually unproven as to the quantitativeness of their measurements' interpretation. In each case, the best estimate of a realistic accuracy or precision is reported.

Chapter three summarizes some examples of remotely sensed data which have value to the OTEC project. The measurements were chosen to be representative of typical data so as not to over-emphasize the best possible results. Workers in satellite oceanography almost always prefer to use positive transparencies on a light table for visual image analysis; the printing process of this technical report markedly degraded the image quality compared to first generation data.

Chapter four is a summary of the technical report. Included after the summary is a glossary of common terms and acronyms in the spacecraft business. The references are the result of a literature search which covers the period 1973-1978 in detail, plus some other frequently quoted references from years before 1973.

## 2.0 SATELLITES AND SATELLITE INSTRUMENTATION OF BENEFIT TO OTEC

### 2.1 SEASAT

#### 2.1.1 Introduction

The SEASAT Program was initiated by the National Aeronautics and Space Administration (NASA) to provide synoptic data on the temperature and dynamic properties of the ocean surface. SEASAT-A was the first satellite in this program and served primarily to demonstrate and validate the measurement capabilities.

The SEASAT-A satellite system was dedicated to the study of the oceanographic environment. The sensors were designed to collect data in the microwave region, thereby providing periodic, near all-weather monitoring of the ocean surface. The instruments on board the SEASAT-A vehicle included: (1) Radar Altimeter, (2) Scatterometer System (SASS), (3) Synthetic Aperature Radar (SAR), (4) Scanning Multifrequency Microwave Radiometer (SMMR), and (5) Visible and Infrared Radiometer (VIR).

The basic orbital characteristics of SEASAT-A are shown in Table 1. The orbit provided for 95 percent global coverage ($\pm 72^{o}$ latitudinal coverage) every 36 hours. However, the swath widths of the SASS, SMMR, and VIR exceeded $\pm 75^{o}$ latitudinal coverage. The altimeter covered $\pm 72^{o}$, but the SAR covered $75^{o}$N to $69^{o}$ because of its right-oriented scan with respect to the satellite's trajectory. Figure 1 illustrates the satellite's trajectory and ground station coverage for SEASAT-A. Data was collected continuously by all instruments, except the SAR. A $4 \times 10^{3}$ bits per second recorder permited global acquisition of all except SAR data. It is important, however, to distinguish between data acquired in near real-time and data used for non real-time applications. Only the readout station at Fairbanks, Alaska (ULA) acquired data for near real-time use

**TABLE 1. BASIC ORBITAL CHARACTERISTICS**

| | |
|---|---|
| Period | 100.75 min |
| Altitude | 794-808 km, nonsun-synchronous |
| Orbits/d | 14.3 |
| Orbit repeat (exact) | 152 d |
| Inclination | 108° |
| Global coverage | ≈ 36 h for 95%. |
| Payload (oceanic sensors) | Microwave radiometer; V&IR radiometer; radar |

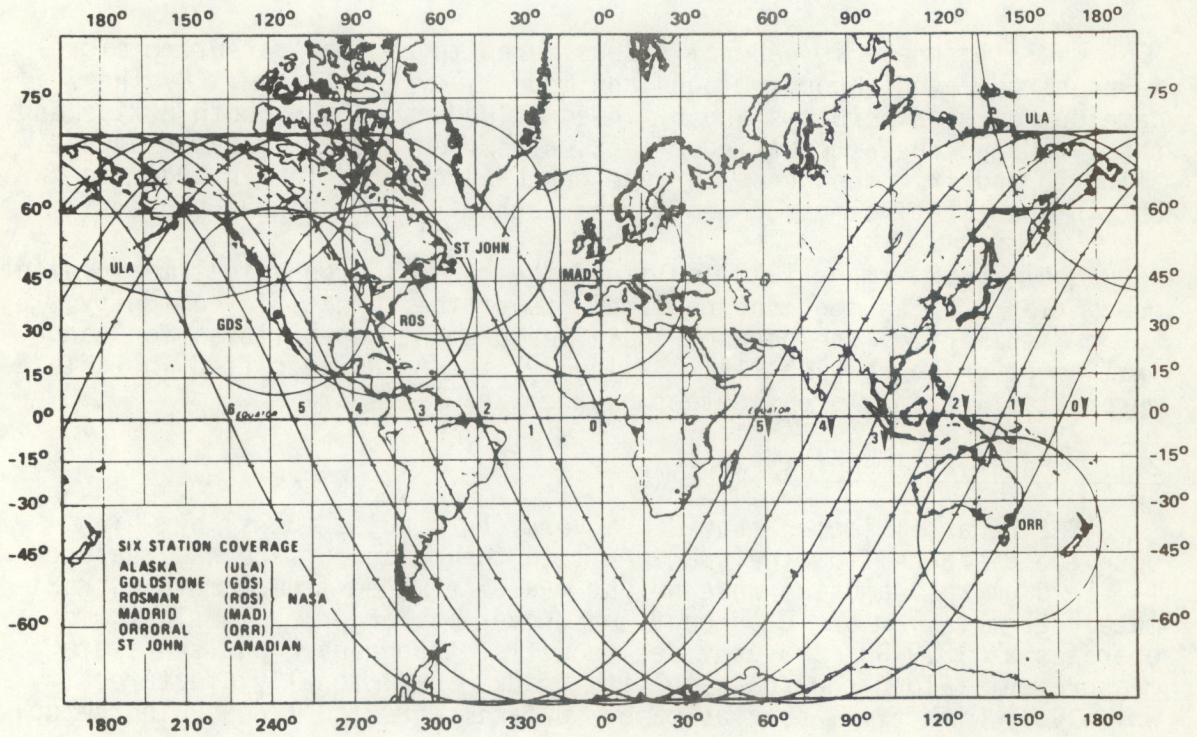


*Figure 1. Typical SEASAT-A ground track trajectories and command and data acquisition (CDA) station coverage. Data from the SAR can be acquired only with the CDA station coverage.*

(up to six hours after initial acquisition by the sensor). Because of the high data rate of the SAR (20 x $10^6$ bits/s) and the orbital characteristics, data from the SAR was not recorded on board and was read out directly at Fairbanks, Alaska, Goldstone, California; Rosman, North Carolina; and St. John, Newfoundland. All of the coastline of the United States, except Hawaii, was to be covered.

### 2.1.2 Instrument Characteristics and Capabilities

Microwave energy interacts with the ocean surface in a somewhat different manner than visible and infrared energy. Microwave energy is influenced by salinity, temperature, angle of incidence (observation), surface roughness, surface containments, atmospheric conditions, and the polarization of the energy. The surface of the ocean involved in the interaction with microwave energy is a function of the distance into the surface in which the initial incident surface value is reduced to 1/e. For example, infrared data reflect a skin depth on the order of tens of micrometers; in the visible region it is tens of meters in clear ocean water; and in the microwave region, it is on the order of centimeters. The specific frequencies of the SEASAT-A instruments and associated skin-depth characteristics provide an alternate view of the ocean surface to that obtained by in-situ instruments and visible or infrared remote sensors.

The atmosphere is generally considered to be transparent to microwave energy, even through clouds and modest levels of rain. By the development of algorithms and by integrating analysis of both active and passive data, the attenuating effects of oxygen and water vapor on radiation to and from the ocean surface can be accounted for in order to obtain quantitative measurements from each of the microwave sensors.

Apel and Sherman (1973) outlined the general geophysical measurement needs (Table 2) to meet the requirements of the scientific community. Table 3 summarizes the oceanographic measurement capabilities for each instrument on board SEASAT-A. Basically, the needs specified in Table 2 were satisfied to a great extent by the SEASAT-A systems.

### 2.1.3 Radar Altimeter

The radar altimeter provided a very short pulse (3 ns) by which both the distance from the spacecraft to the ocean surface was measured ($\leq \pm$ 20 cm rms) and the wave height was determined from 1 m to approximately 25 m ($\pm$ 1 m or 10 percent, whichever is larger). The instrument operates at 13.9 GHz and provided geodetic, topographic and sea-state measurements along the sub-satellite track. Additionally, features which vary with time, such as major surface currents, tides, wind setup, and storm surges were to be detected.

The altimeter had a nadir looking (only) antenna with a spatial resolution of 1.6 to 12.0 km. The spatial resolution was determined not by the beam width of the antenna but by the compressed pulse length of 3 ns. The important point to note is that data was only obtained along

**TABLE 2. GEOPHYSICAL OCEANOGRAPHIC MEASUREMENT NEEDS**

| MEASUREMENT | | | RANGE | PRECISION/ ACCURACY | RESOLUTION | SPACIAL GRID | TEMPORAL GRID |
|---|---|---|---|---|---|---|---|
| Topography | Geoid | | 5cm-200m | <±10cm | <10km | | Weekly to monthly |
| | Currents, surges, etc. | | 10cm-10m<br>5-500cm/s | <±10cm<br>±5cm/s | 10-1000m | <10km | Twice a day to weekly |
| Surface Winds | Amplitude | Open ocean | | | 10-50km | 50-100km | 2-8/d |
| | | Closed sea | 3-50m/s | ±1 to 2m/s or ±10% | 5-25km | 25km | |
| | | Coastal | | | 1-5km | 5km | Hourly |
| | Direction | | 0-360° | ±10-20° | | | |
| Gravity Waves | Height | | 0.5-20m | ±0.5m or ±10-25% | <20km | | 2-8/d |
| | Length | | 6-1000m | ±10-25% | | <50km | |
| | Direction | | | ±10-30° | 3-50m | | 2-4/d |
| Surface Temperature | Open sea | | | | 25-100km | 100km | Daily to weekly with spectrum of times of day and times of year |
| | Closed sea | | –2-35°C | 0.1-2° relative<br>0.5-2° absolute | 5-25km | 25km | |
| | Coastal | | | | 0.1-5km | 5km | |
| Sea Ice | Extent and age | | | 1-5km | 1-5km | 1-5km | Weekly |
| | Leads | | >50m | 25m | 25m | 25m | 2-4/d |
| | Icebergs | | >10m | 1-50m | 1-50m | | |
| Ocean Features | Open ocean | | | 50-500m | | | Twice daily to daily |
| | Coastal | | | 10-100m | | | |
| Salinity | | | 0-30ppt | ±0.1-1ppt | 1-10km | 100km | Weekly |
| Surface Pressure | | | 930-1030mb | ±2-4mb | 1-10km | 1-10km | Hourly |

**TABLE 3. GEOPHYSICAL OCEANOGRAPHIC MEASUREMENT CAPABILITIES FOR SEASAT-A**

| MEASUREMENT | | | RANGE | PRECISION/ ACCURACY | RESOLUTION km | SPACIAL GRID | TEMPORAL GRID |
|---|---|---|---|---|---|---|---|
| Topography | Geoid | Altimeter | 5cm-200m | <±20cm | 1.6-12 | ~10 | Less than 6 months |
| | Currents, Surges, etc. | | 10cm-10m | | | | |
| Surface Winds | Amplitude | Microwave Radiometer | 7-50m/s | ±2m/s or ±10% | 50 | 50 | 36h to 95% Coverage |
| | Amplitude | Scatter-ometer | 3-25m/s | ±2m/s or 10% | 50 | 100 | 36h to 95% Coverage |
| | Direction | | 0-360° | ±20° | | | |
| Gravity Waves | Height | Altimeter | 0.5-25m | ±0.5 to 1.0m or ±10% | 1.6-12 | Nadir only | 1/14d near Continental U.S. |
| | Length | Imaging Radar | 50-1000m | ±10% | 50m | | |
| | Direction | | 0-360° | ±15% | | | |
| Surface Temperature | Relative | V&IR Radiometer | -2-35° C Clear weather | 1.5° | ~5 | ~5 | 36h |
| | Absolute | | | 2° | | | |
| | Relative | Microwave Radiometer | -2-35° C All weather | 1° | 100 | 100 | 36h |
| | Absolute | | | 1.5° | | | |
| Sea Ice | Extent | V&IR Radiometer | | ~5km | ~5 | ~5 | 36h |
| | Extent | Microwave Radiometer | | 10-15km | 10-15 | 10-15 | 36h |
| | Leads | Imaging Radar | >50m | ±25m | 25m | | 1/14d near Continental U.S. |
| | Icebergs | | >25m | ±25m | 25m | | |
| Ocean Features | Shores, Clouds, Islands | V&IR Radiometer | | ~5km | ~5 | ~5 | 36h |
| | Shoals, Currents | Imaging Radar | | ±25m | 25m | 25m | 1/14d near Continental U.S. |
| Atmospheric Corrections | Water Vapor & Liquid | Microwave Radiometer | | ±25m | 50 | 50 | 36h |

the sub-point track of the satellite. Therefore, spatial analysis required integration of data from a large number of orbital passes (the order of a month long period) over a given area. This limited spatial analyses to ocean features which do not vary appreciably with time (e.g., the Loop Current).

There was a need to correct various errors that arose in the data. One such error was due to a shift away from the mean sea-level position toward the troughs of waves. This shift increases as the surfaces becomes rougher. Because of the importance of this error, the altimeter was designed to be self-correcting. Corrections for the microwave index of refraction of the atmosphere were necessary, in order to attain the expected accuracy of $< \pm 20$ cm. These corrections were made using the microwave radiometer measurements. The microwave radiometer measurements were critical to the altimeter accuracy, and so the utility of the altimeter data was strongly dependent on maintaining an operational microwave radiometer.

The altimeter measurements yielded the summation of the satellite height above a reference spheroid, the local geoid height, and a departure of height brought about by oceanic perturbations. In order to obtain the oceanographic signal, the satellite height and the local geoid height must be known. The satellite height was determined by the satellite tracking data; however, to date, no accurate analysis of the geoid height distribution exists for the Gulf of Mexico. Until such an analysis is developed, the utility of the altimeter data to study oceanic features in the Gulf is extremely limited.

It is expected that given all required a priori data and after all corrections have been made, the data can be used to study major current systems (such as the Gulf Loop Current) having velocities greater than 30 cm/sec, tides, wind set-up, and storm surges. It may also be possible to study the variations of the features with time in small spatial intervals. This system was to provide data in specific phenomena such as hurricanes and sea-state conditions in other major storms which were impossible to obtain in the past.

### 2.1.4 Scatterometer

The SEASAT-A Scatterometer System (SASS) was an active sensor designed primarily to serve as a low to intermediate wind velocity anemometer. It operated at 13.9 or 14.595 GHz and measured surface roughness as a function of wind with an accuracy of $\pm$ 2 m/s or 10% (whichever was larger) and $\pm 20^{o}$ in direction. The range of the wind speed measurements was from about 3 m/s to potentially 25 m/s. The swath coverage of the system on the earth's surface was 1000 km with a ground resolution of 50 km at nadir. Global coverage was accomplished in 36 hours.

This system might have provided data for the spatial distribution of the surface wind velocity over an area the size of the Gulf of Mexico at least once every two days. Wind measurements might have been obtained as

close as 60 km from the coast. Observations obtained closer to the coast may have been contaminated by the coastal ground cover. These observations were, therefore, most useful for large bodies of water such as open oceans, Gulf of Mexico, Indian Ocean, etc.

The analysis of the spatial distribution of the winds in given synoptic weather states can be used to study the effect of synoptic-scale weather systems on major current systems, on the production and modification of oceanic eddies, on the production and/or enhancement of secondary ocean currents, etc. The data could have been used to determine the distribution of along-shore winds and the distribution of curl of the surface wind stress, both of which are important in understanding oceanic energetics. In essence, these data could have been used to study one of the primary forcing functions governing the behavior of the ocean - the surface wind stress. These data could be beneficial to enhancing our understanding of mechanisms responsible for, of the frequency of occurrence of, and of the movement of oceanic perturbations that may be detrimental to the operation of an OTEC in a given region.

### 2.1.5 Synthetic Aperature Radar

The Synthetic Aperature Radar (SAR) was designed to provide 25 m spatial resolution images and wave directional spectra over a 100 km swath width. The 25 m spatial resolution of the SAR only allowed for the discrimination of gravity waves having wavelengths of 50 m or more. The SAR operated at 1.37 GHz and had excellent cloud and rain penetration capability. The orbital characteristics of SEASAT-A provided for SAR orbit repeat every 152 days, but a given surface feature observed in a SAR image might have been seen for several consecutive days every 70 days.

The data from the SAR was collected only in a direct readout mode. The data rate of $20 \times 10^6$ bits/s prohibited on-board recording. On the average, images for a given area were to be obtained once every 18 days and only in the vicinity of a readout station. This limited data collection to the oceanic regions near the continental North America. Relative to the regions of interest to OTEC, data from the SAR was only provided for the Gulf of Mexico.

As indicated above, the SAR could function through clouds and nominal rain to provide wave patterns, high resolution images of sea and lake ice, ocean pollution of the surface such as oil spills, current patterns manifested by wave modification, internal wave patterns, storm damage to coast lines, and fishing vessel surveillance. These data could be used to study wave energy convergence and dissipation, wave spectra ( in two dimensions), the interaction of waves with shoals, and the interaction of waves at the boundary of water masses. They could also be used to develop and verify wave models.

Of interest to OTEC was the potential to establish mean wave spectra at potential OTEC sites to determine the wave energy OTEC will be exposed to at those sites. Such information is important in screening OTEC sites.

Also, the SAR could have been used to monitor certain aspects of the impact of OTEC on the environment because of its capability to monitor certain forms of ocean pollution. It could have also been possible to determine more precisely the position of the Loop Current through wave characteristics at water mass boundaries. In the past, satellite infrared imagery has provided a reasonable indication of the Loop Current's position; but under certain circumstances, these data can be misleading.

### 2.1.6 Microwave Radiometer

The Scanning Multi-frequency Microwave Radiometer (SMMR) was to provide global coverage every 36 hours in the area bounded by $\pm 72^{o}$ latitude. The five operating frequencies (6.6, 10.69, 18.0, 22.05 and 37.0 GHz) of the SMMR were to enable the sensor to serve as an intermediate to high windfield anemometer (wind speeds ranging from 7 to 50 m/s) and to measure brightness temperature relative to atmospheric corrections for liquid and water vapor, sea-surface temperature and ice fields. The along-track and cross track resolution depended on the frequency. For 6.6 GHz, the along-track resolution was 144 km and the cross track resolution was 92 km; for 10.69 GHz, 89 km and 57 km, for 18.0 GHz, 53 km and 34 km; for 22.05 GHz, 43 km and 29 km; and for 37.0 GHz, 26 km and 17 km.

Each frequency was sensitive to a different environmental parameter. The 6.6 GHz frequency was most sensitive to surface temperature; the 10.69 GHz and the 18.00 GHz frequencies, to atmospheric water vapor; and the 37 GHz frequency, to sea ice conditions. Of these parameters, only surface temperature, surface roughness, and water vapor data had any immediate utility to the OTEC program.

The microwave radiometer could detect surface temperature even through certain clouds, a factor not possible using infrared systems. However, the data from the microwave system had limited use because the resolution (~ 100 km) did not yield a precise definition of temperature in specified locations. Infrared systems have considerably better resolution (~ 1 km to 8 km). Perhaps the best use of the microwave temperature data would be to supplement the infrared data in regions of cloudiness.

Since the surface roughness is proportional to surface stress and the surface wind field, the 10.69 and 18.0 GHz data could have been used to obtain these data. However, the fact that no directional information was obtained indicates that these data are best used to supplement the scatterometer data. The water vapor data from the 22.05 GHz frequency could have been used to study the impact of OTEC on the flux of water vapor from the ocean surface. A potential impact may arise due to mixing of the cold subsurface water with the surface water lowering the surface temperature of the ocean. This will reduce the flux of water vapor from the surface, and may have a direct bearing on changing downwind weather conditions.

### 2.1.7 Visible and Infrared Radiometer

The Visible and Infrared Radiometer (VIR) was a modified version of the Scanning Radiometer (SR) flown on the NOAA operational satellites. The two channels (0.52 - 0.73 μm and 10.5 - 12.5 μm) provided day and night coverage of both cloud conditions and major oceanic thermal features. The VIR data was to be used principally for feature identification and as a comparative observation of sea-surface temperature to the SMMR temperature data. However, since the visible and infrared data could have been used to detect ocean fronts through sunglint effects in regions of different surface roughness and through the surface temperature, these data would have been part of a large body of such data which will be available for OTEC purposes.

### 2.1.8 Applicability of SEASAT-A to OTEC Resource Assessment and Monitoring

A basic need of the OTEC Resource Assessment and Monitoring Program is a better understanding of oceanographic phenomena and their aerial distribution. Observations of sufficient scope, distribution, frequency, and detail are fundamental to an improved environmental analysis and subsequent predictable behavior. Current knowledge of the oceanographic and seashore areas is based primarily on data derived from observations made along the primary shipping lanes or intermittent special investigation surveys. With the exception of cloud information, sea ice, sea surface temperature, and atmospheric sounding data obtained by the operational NOAA series satellites, most of the oceans are not routinely monitored.

The microwave sensors of SEASAT-A were expected to provide timely synoptic data of the surface wind fields, waves, storm surge and setup. The improved geoid data would have contributed directly to a refined definition of a standard reference surface for the oceans which would enhance derivation of currents, sea slope, ocean tides, and sea state.

During the demonstration and experimental phase of SEASAT-A, there was a significant increase in observational data. This increase in aerial and temporal observational data contributed to improved understanding, description, and prediction services in marine meteorology and oceanography. However, it is not clear to what degree data from SEASAT and future satellites having instrumentation similar to SEASAT will contribute to improved understanding and predictive capability. It is important that these data be employed in oceanographic studies in potential OTEC sites to determine their applicability. This aspect is crucial to monitoring the meso- and synoptic-scale oceans when OTEC is in an operational phase.

## 2.2 TIROS-N

The first two satellites of the TIROS-N series will carry new environmental monitoring instruments which represent major technological advances over those on board the ITOS series satellites they will replace. Following the successful launch of TIROS-N in October 1978, program plans call for the two TIROS-N systems to be launched to insure uninterrupted polar environmental satellite services. The two satellites will allow six hourly coverage of a specified area. Four pairs of the TIROS-N third generation satellite are planned in order to provide continuing service through 1986. The design of the TIROS-N satellite provides for an operational lifetime of two years, and a potential growth of up to 25 percent in terms of weight, volume, power, command and telemetry capabilities.

The initial TIROS-N satellite will be placed into an afternoon orbit with a 1500 local ascending node time. The orbit will be near polar and sun synchronous at an average altitude of 540.6 miles (870 km). The orbital period will be 101.6 minutes, thus allowing 14.12 orbits per days. The second satellite, NOAA-A, will be placed at an average orbital altitude or 517.6 miles (833 km) with an equator crossing descending at 0730 local time.

### 2.2.1 Instruments

The four primary instruments on board the TIROS-N satellites are the Advanced Very High Resolution Radiometer (AVHRR), the TIROS Operational Vertical Sounder (TOVS), the Data Collection System (DCS), and the Space Environment Monitor (SEM). Of these four instrument systems, the AVHRR and DCS can make a significant contribution to a program of assessment and monitoring of potential ocean thermal resources.

### 2.2.2 Advanced Very High Resolution Radiometer (AVHRR)

The AVHRR will provide image data for real-time transmission to both Automatic Picture Transmission (APT) and High Resolution Picture Transmission (HRPT) stations. The data will be available in four operational modes:

(1) Direct readout to receiving stations of the APT class, worldwide, a 4 km resolution, of the visible and infrared data, with panoramic distortion removed from any two spectral channels (wavelengths).

(2) Direct readout to receiving stations of the HRPT class, worldwide, at 1.1 km resolution of all spectral channels.

(3) Global on-board recording of 4 km resolution data from all spectral channels for commanded readout.

(4) On-board recording of data from selected portions of each orbit at 1.1 km resolution of all spectral channels.

The AVHRR instrument for TIROS-N is sensitive to four different spectral wavelengths. A planned design change in the instrument in 1980 will incorporate a fifth spectral wavelength of sensitivity 11.5 - 12.5 μm. Table 4 summarizes the sensitivity characteristics of the AVHRR instrument.

**TABLE 4. TIROS-N AVHRR CHANNEL CHARACTERISTICS**

| CHANNEL* | RESOLUTION AT SUBPOINT | WAVELENGTH (μm) | PRIMARY USE |
|---|---|---|---|
| 1 | 1 km | 0.55 - 0.90 | Daytime cloud and surface mapping |
| 2 | 1 km | 0.725 - 1.10 | Surface water delineation |
| 3 | 1 km | 3.55 - 3.93 | SST, nighttime cloud mapping |
| 4 | 1 km | 10.5 - 11.5 | SST, day/night cloud mapping |
| 5 | 1 km | 11.5 - 12.5 | SST |

*Channel 1 wavelength will be 0.58-0.68μm for *all* instruments after the TIROS-N flight model. Channel 4 wavelength will be 10.3-11.3μm for all AVHRR/2 instruments. Channel 5 will not be on early AVHRR/1 flights but will be added with the AVHRR/2 instrument to further enhance Sea Surface Temperature (SST) measurements in the tropics.

As shown in Table 4, channels 1 and 2 will be used to identify clouds, land-water boundaries, snow and ice. These data may also be useful in determining ocean fronts through differences in surface scattering. The data received from Channel 4 will be sensitive cloud radiation during the day and the night, and will be useful in determining cloud temperature and distribution. Channels 3, 4 and 5 are important to oceanographic studies and monitoring programs. Channels 3 and 4 will be used to determine the sea-surface temperature. The integration of these two channels will provide the ability to remove any ambiguity introduced by clouds covering a portion of the field of view and correcting for atmospheric absorption. However, it should be noted that Channel 3 will provide sea-surface temperature data only at night because this channel is contaminated by reflected solar radiation in the daytime. Therefore, corrections can only be applied to nighttime data.

Channel 5, to be included in the AVHRR/2 instrument, will further enhance sea-surface temperature measurements in tropical areas. It is anticipated that the sensitivity of Channel 5 will be extremely valuable in the subtropical and middle latitudes also, especially during the summer months when intense surface heating tends to mask the surface manifestations of the ocean's thermal structure. These data will also yield increased thermal detail at the surface in important warm ocean currents (e.g., Gulf Stream, Loop Current, etc.).

### 2.2.3 Data Collection System

The DCS instrument on board TIROS-N, provided by the Centre National d'Etudes Spatiales (CNES) of France is known as the ARGOS Data Collection and Platform Location System. The ARGOS DCS will provide a means to locate and/or collect data from fixed and free-drifting buoy and balloon platforms. When the TIROS-N system is fully operational (e.g., two satellites in ascending and descending orbital configuration), a given platform will be in contact with the spacecraft at least four times each day. These intervals will be approximately six hours apart. During any interval, the platform will be received by the spacecraft on at least two successive orbits, which would provide a minimum of eight reports a day. The location information is determined by measuring the platform carrier frequency received by the DCS instrument at each transmission and using differential doppler techniques to calculate the platform location with an accuracy of 3-5 km RMS.

The ARGOS system will receive data from the various platforms at UHF (401.65 MHz). The platforms will transmit independently of any interrogations from the spacecraft which uses a random access receiving system. The platforms will make continual transmissions which will vary in length from 360 to 920 ms with a repetition interval from 40 to 200 seconds. When the spacecraft comes within range of a platform, it will receive and record the data. Later, the data is transmitted to a Command and Data Acquisition (CDA) station. The platform locations are determined through on the ground processing. Buoy locations can be used to determine trajectories and currents associated with oceanic perturbations. Such data can be useful to OTEC requirements.

The ARGOS system will also provide for the immediate rebroadcast of data received from the platforms. Such data may include surface and subsurface temperature and salinity data, current data, etc. Only data from platforms so located that both the platform and the receiving site are simultaneously in view of the satellite will be available for this rebroadcast.

### 2.2.4 Applicability of TIROS-N to OTEC Resource Assessment and Monitoring

The AVHRR system aboard the TIROS-N satellite will provide synoptic scale analyses of thermal boundaries associated with major ocean currents, oceanic eddies, and other such phenomena. The applicability of such data to OTEC resources assessment and monitoring has been demonstrated in the past (Vukovich et al., 1978). However, the potential that this system will provide an accurate quantitative measure of the sea surface temperature as well as a qualitative measure is very important.

The OTEC resource is generally based on the temperature differences between the surface and the subsurface (~ 1000 m depth). Wolf et al. (1977) have shown that the temperature variability at the 1000 m depth is small (~ 2°C), so that the variability of the OTEC resource is governed by the variability of the temperature in the near surface layer. Therefore, synoptic-scale, sea-surface temperatures can be utilized to

predict the expected variability of the resource, a factor of critical importance to OTEC operation. Since, however, the warm-water intake for OTEC is below the sea-surface, but within the first 100 m, correlation studies are required between the variability of the sea-surface temperature as detected by the satellite, the temperature in the surface layer (~ 50 m depth), and the OTEC resource (the temperature difference between the 50 m depth and the 1000 m depth, for instance).

The primary use of the Data Collection Systems on TIROS-N for OTEC purposes should be the detection of current systems that may influence OTEC operations. Ocean thermal perturbations detected by a satellite's radiometer generally have associated with them current systems. These currents could affect the mooring stability of an OTEC and the diffusion and transport of water mass discharged from the OTEC. The strength of these currents can best be established by placing a free drifting buoy which can be tracked by the ARGOS system on TIROS-N, in a position prescribed by the infrared imagery. Techniques for deployment of the buoys by aircraft should be established because ship deployment is time consuming and costly. Buoy deployment can be manifested before the perturbation influences the OTEC to predict potential effects, and during the period the perturbation is influencing the OTEC to establish actual effects. Some a priori information ascertained by studying the current systems of perturbations which may influence OTEC in the region of interest by deployment of free drifting buoy in case studies, may preclude deployment of buoys after OTEC has been deployed, if correlations can be found between surface isotherms patterned from satellite infrared measurements, altimetry measurements, and other pertinent satellite data with surface current data. Such correlations may exist in the case of oceanic perturbations.

## 2.3 NIMBUS 7

### 2.3.1 Introduction

The NIMBUS satellite program was initiated by NASA in the early 1960's. Since then, the project has become the nation's principle satellite program for remote sensing research. The NIMBUS 7 mission provides the opportunity to conduct a variety of experiments in the oceanographic and meteorological disciplines.

NIMBUS 7 was launched in October, 1978 and assumed a circular sun synchronous orbit. The subsatellite track pattern nearly repeats itself every four days. Additional orbit parameters are shown in Table 5.

### 2.3.2 Instruments

The instrument payload on board NIMBUS 7 includes: (1) Coastal Zone Color Scanner (CZCS), (2) Earth Radiation Budget (ERB), (3) Limb Infrared Monitor of the Stratosphere (LIMS), (4) Stratospheric Aerosol Measurement II (SAM II), (5) Stratospheric and Mesospheric Sounder (SAMS), (6) Solar and Backscattered Ultraviolet/Total Ozone Mapping Spectrometer (SBUV/TOMS), (7) Scanning Multichannel Microwave Radiometer (SMMR), and (8) Temperature Humidity Infrared Radiometer (THIR). An instrument summary is shown in Table 6.

## TABLE 5: BASIC ORBITAL CHARACTERISTICS OF NIMBUS-7

| | |
|---|---|
| **Nominal Orbit Parameters** | |
| Altitude | 955 Km |
| Inclination | 99.2° |
| Period | 104.15 minutes |
| Orbits per day | 13.82 (results in daily ascending node separation of 4.55°) |
| Ascending node separation for adjacent orbits | 26.04° (Westward motion) |
| **Launch Parameters** | |
| Ascending node time | 11:52 |
| Date | Nov 25, 1978 |
| Resulting Sun Angle | 8° |

Table 6: NIMBUS-7 Instrument Summary

| Instrument | Type of Device | Parameter Determinations | Discipline |
|---|---|---|---|
| LIMS - Limb Infrared Monitor of the Stratosphere | Limb Scanning Infrared Radiometer | $H_2O$, $HNO_3$, $NO_2$, $O_3$, Temperature - Vertical Profiles | Pollution, Meteorology |
| SAMS - Stratospheric and Mesospheric Sounder | Limb Scanning Pressure Modulated Infrared Radiometer | $CH_4$, CO, $H_2O$, NO, $N_2O$, Temperature - Vertical Profiles | Pollution, Meteorology |
| SAM II - Stratospheric Aerosol Measurement | Solar Extinction Photometer, Limb Viewing | Aerosols - Vertical Profiles | Pollution, Meteorology |
| SBUV/TOMS - Solar and Back-scattered Ultraviolet/Total Ozone Mapping Spectrometer | Sun and Earth Viewing Monochromators, Nadir Viewing and Nadir Scanning | Solar UV Irradiance, Ozone Profiles, Global Maps of Total Ozone | Pollution, Meteorology |
| ERB - Earth Radiation Budget | Sun and Earth Viewing Spectroradiometer, Nadir Viewing and Nadir Scanning | Solar Irradiance, Flux and Radiance of Earth Reflected Short-wave and Emitted Long-wave Radiation | Meteorology |
| SMMR - Scanning Multichannel Microwave Radiometer | Earth Viewing Microwave Radiometer, Conical Scanning | Sea Ice, Sea Surface Temperatures and Winds, Cloud Liquid Water Content, Precipitation, Water Vapor, Soil Moisture, Snow Cover | Oceanography, Meteorology Hydrology Climatology |
| CZCS - Coastal Zone Color Scanner | Earth Viewing Radiometer Nadir Scanning | Chlorophyll, Sediment Distribution, Gelbstoffe Concentration (Salinity), Coastal Water Temperature, Currents | Oceanography, Meteorology |
| THIR - Temperature Humidity Infrared Radiometer | Earth Viewing Infrared Radiometer, Nadir Scanning | Correlative Imagery for Other Experiments, Sea Surface Temperature Patterns | Supports All Discipline Investigations |

The CZCS, SMMR and THIR instruments appear to be useful to an OTEC resource assessment and monitoring program. Each of these instruments will be discussed in detail.

### 2.3.3 Coastal Zone Color Scanner

The CZCS is the first instrument flown on a spacecraft that will be devoted to ocean color. Every parameter has been optimized for use over water to the exclusion of any other type of sensing. The objective is to map chlorophyll concentration, sediment distribution, Gelbstoff concentration, and temperatures of coastal waters and the open ocean.

The CZCS scans six spectral bands; five sense backscattered solar radiance, and the sixth senses emitted thermal radiance. Bands one through four are used for water color determination, band five is useful for discriminating land features, and the sixth band operates in the infrared to measure equivalent blackbody temperature. Table 7 summarizes the CZCS performance parameters. Algorithms relating one or more of these radiance measurements to some physical property, such as phytoplankton or suspended sediment concentrations, are already available.

The CZCS has considerable built-in flexibility in order to accomodate a wide range of conditions. Examples are: (1) Variable gain in channels one through four - gain may be changes in order to utilize the best dynamic range possible without saturating over-water targets. (2) Scan mirror tilt - the scanning mirror may be angled to look either forward or behind the spacecraft in two degree increments, up to twenty degrees in either direction. This feature reduces sunglint problems. (3) Contrast enhancement through signal offset; a DC offset can adjust the measured radiance of the first four channels. The entire digital range of the digitizer is then used to cover only that part of the signal containing modulation due to change in ocean color. This feature reduces the effect of radiation backscattered by the atmosphere.

It is important to realize that the CZCS operation is limited by spacecraft power to approximately two hours per day. Operation will be in two minute segments over areas chosen by the NIMBUS Experiment Team. The United States coastline, and the coastlines of Europe and South Africa presently have a high priority for continuing coverage.

CZCS data will be available on tape or in the form of a photographic image (see Figure 2). A maximum of 22,000 images per year may be generated, but cloud cover will probably reduce output to approximately 12,000 images. Each image of channel one through four covers six degrees latitude by five degrees longitude (near midlatitude). Channel five and six images cover seven by twelve degrees.

### 2.3.4 Scanning Multichannel Microwave Radiometer

The NIMBUS 7 SMMR is a five band passive microwave imager. Separable horizontal and vertical polarization components create a total of ten channels of radiometric data. Determination of parameters useful to OTEC include ocean surface wind stress and sea surface temperature. The

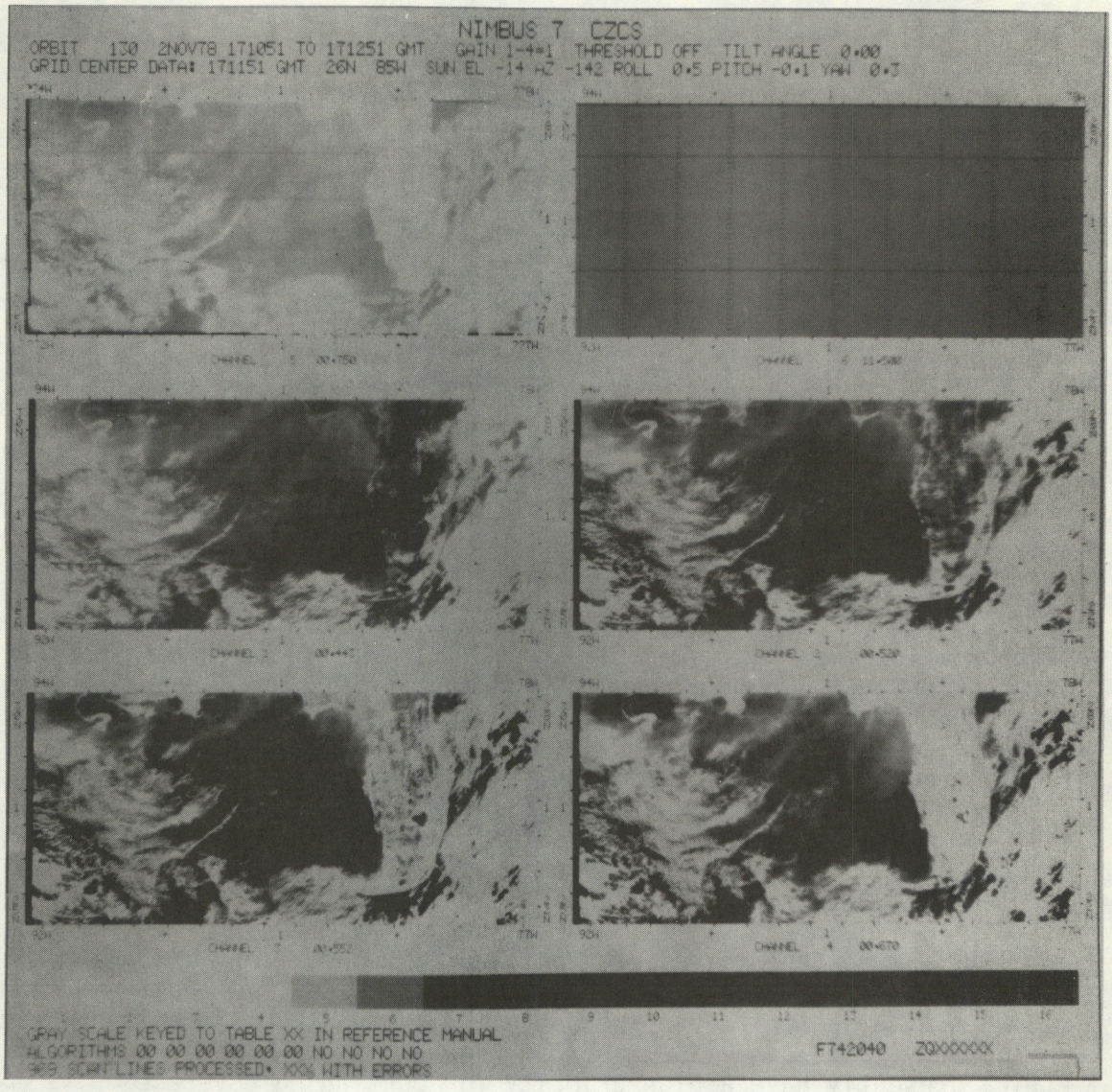


*Figure 2. Film data format from the coastal zone color scanner aboard the NIMBUS 7 spacecraft. No emitted infrared (10.5-12.5 μm) data were observed in this pass. Area covered is identical to that in Figure 8, the northeastern Gulf of Mexico (W. Hovis, personal communication).*

Table 7: CZCS Performance Parameters

| Performance Parameters | Channels | | | | | |
|---|---|---|---|---|---|---|
| | 1 | 2 | 3 | 4 | 5 | 6 |
| Scientific Observation | Chlorophyll Absorption | Chlorophyll Correlation | Yellow Stuff | Chlorophyll Absorption | Surface Vegetation | Surface Temperature |
| Center Wavelength λ Micrometers | 0.443 (blue) | 0.520 (green) | 0.550 (yellow) | 0.670 (red) | 0.750 (far red) | 11.5 (infrared) |
| Spectral Bandwidth Δλ Micrometers | 0.433 – 0.453 | 0.510 – 0.530 | 0.540 – 0.560 | 0.660 – 0.680 | 0.700 – 0.800 | 10.5 – 12.5 |
| Instantaneous Field of View (IFOV) | ← 0.865 x 0.865 Milliradians (0.825 x 0.825 km at sea level) → | | | | | |
| Co-registration at NADIR | <0.15 Milliradians | | | | | |
| Accuracy of Viewing Position Information at NADIR | <2.0 Milliradians | | | | | |
| Signal to Noise Ratio (min.) at Radiance Input N< (mW/cm$^2$ · STER · μm) | >150 at 5.41 | >140 at 3.50 | >125 at 2.86 | >100 at 1.34 | >100 at 10.8 | NETD of 0.220°K at 270°K |
| Consecutive Scan Overlap | 25% | | | | | |
| Modulation Transfer Function (MTF) | 1 at 150 km target size, 0.35 min. at 0.825 km target size | | | | | |

outstanding feature is the nearly all-weather capability of the system. Spatial resolution varies from about 20 KM to 150 KM, depending upon wavelength. Additional SMMR performance characteristics are found in Table 8.

The SMMR operates on a 50% duty cycle in order to conserve spacecraft power. For time series analyses, the duty cycle is achieved by operating on alternate days throughout its functional lifetime. This constraint reduces scan overlap, but the entire earth will still be mapped every six days.

Algorithms for sea surface temperature and sea surface wind speed have already been delivered. These will be refined during instrument validation. SMMR data will be available in a variety of tape and display products. Probably the most useful for OTEC analysis will be the mercator projection maps. At best, these maps will have a resolution of 25 km and will be produced every three days.

### 2.3.5 Temperature-Humidity Infrared Radiometer

The THIR on NIMBUS 7 is of the same design and operation as the THIR flown on NIMBUS 4, 5, and 6. Although the radiometer is a two channel instrument, only the 11.5 μm band provides a useful temperature map of the ocean surface. The resolution at the satellite subpoint is 6.7 km for this band. The deterioration of this resolution is depicted in Figure 3. Additional specifications are given in Table 9.

The THIR data is available on tape or as a display product. This display product, a 9.5 inch square block and white print, is available twice daily (night and day images).

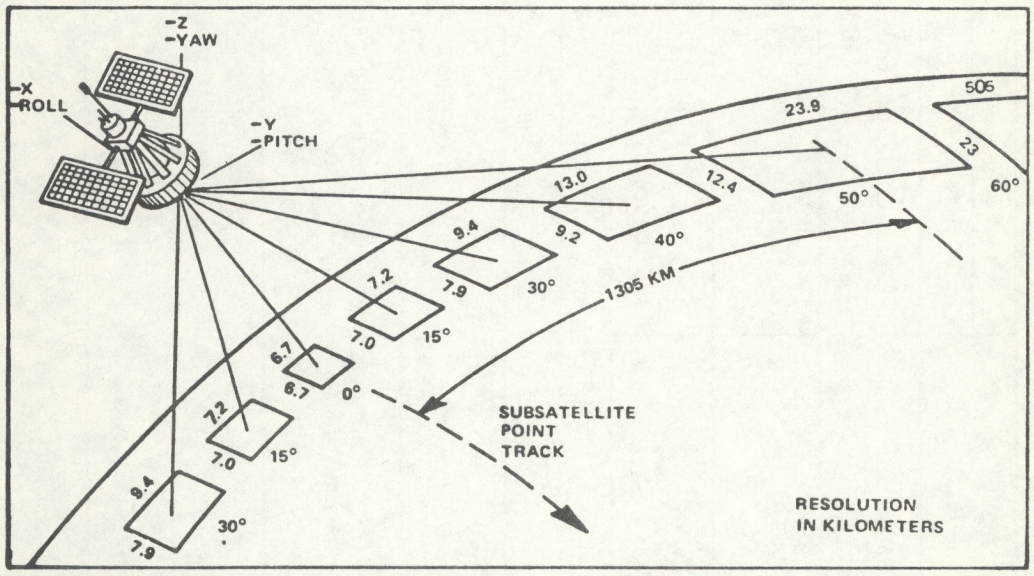


*Figure 3. Schematic drawing of resolution of the THIR aboard the NIMBUS 7 spacecraft. The nadir angle is given with each resolution element; i.e., at 30° nadir angle, the picture element is 7.9 km x 9.4 km (from NIMBUS 7 User's Guide).*

Table 8: SMMR Performance Characteristics

| Parameter | Channel | | | | |
|---|---|---|---|---|---|
| | 1 | 2 | 3 | 4 | 5 |
| Wavelength (cm) | 4.54 | 2.8 | 1.66 | 1.36 | 0.81 |
| Frequency (GHz) | 6.6 | 10.69 | 18.00 | 21.00 | 37.00 |
| R-F Bandwidth (MHz) | 250 | 250 | 250 | 250 | 250 |
| Integration Time (ms) (approximate) | 126 | 62 | 62 | 62 | 30 |
| I-F Frequency Range (MHz) | 10-110 | 10-110 | 10-110 | 10-110 | 10-110 |
| Dynamic Range (°K) | 10-330 | 10-330 | 10-330 | 10-330 | 10-330 |
| Absolute Accuracy (°K rms) | <2.0 | <2.0 | <2.0 | <2.0 | <2.0 |
| Temperature Resolution, ΔTrms (°K) (per IFOV)* | 0.9 | 0.9 | 1.2 | 1.5 | 1.5 |
| Antenna Beam Width (±0.2°) | 4.2 | 2.6 | 1.6 | 1.4 | 0.8 |
| Antenna Beam Efficiency (percent) | 87.0 | 87.0 | 87.0 | 87.0 | 87.0 |
| Scan Cycle ±0.4 rad (±25°)/second** | 4.096 | 4.096 | 4.096 | 4.096 | 4.096 |
| Double Sideband Noise (dB) (maximum) | 5.0 | 5.0 | 5.0 | 5.0 | 5.0 |

*IFOV are remapped to form equal sized cells (150, 90, 50km) across the swath prior to retrieval of geophysical parameters; the ΔT rms's are correspondingly lower.

**Add 2 ms (used for integer dump) for complete IFOV cycle time.

Table 9: THIR Subsystem Specifications

| Design Parameter | Channel 1 | Channel 2 |
|---|---|---|
| Wavelength Band of Operation (Half Power Points (microns)) | 6.5 to 7.0 | 10.5 to 12.5 |
| Field-of-View (mrad) | 20 | 7 |
| Ground Resolution (Subsatellite Point at 955 Km) (Km) | 20 | 6.7 |
| Collecting Aperture ($cm^2$) | 110 | 110 |
| Detector (Immersed Bolometer) | | |
| Size (mm) | 0.67 x 0.67 | 0.22 x 0.22 |
| Time Constant (msec) | 2.7 | 1.8 |
| Scan Rate (rps) | 0.8 | 0.8 |
| Dwell Time (msec) | 4.2 | 1.4 |
| Information Bandwidth (Hz) | 115 | 345 |
| Dynamic Range (Target Temperature) (°K) | 0 to 270 | 0 to 330 |
| **Performance Characteristics** | **Channel 1** | **Channel 2** |
| Noise Equivalent Irradiance (NEI) ($watts/cm^2$) | $4.35 \times 10^{-10}$ | $3.0 \times 10^{-10}$ |
| Noise Equivalent Temperature Differential (NETD) at Indicated Scene Temperature | 5.0°K @ 185°K<br>0.26°K @ 300°K | 1.5°K @ 185°K<br>0.28°K @ 300°K |
| S/N Ratio at Indicated Scene Temperature | 3.8:1 @ 185°K<br>110:1 @ 270°K | 19:1 @ 185°K<br>375:1 @ 330°K |
| **Physical Characteristics** | **Scanner** | **Electronics Module** |
| Weight (lbs) | 14.0 | 6.0 |
| Size (in.) | 7.5 x 7.1 x 15.7 (Excluding sunshield) | 7.0 x 6.8 x 6.0 |
| **Power Requirements** | **Scanner** | **Electronics** |
| -24.5 vdc (watts) | 1.8 | 5.8 |
| 100-Hz Two-Phase Square Wave 5.25 V (watts/phase) | 0.1 | |
| **Operating Temperature Range** | **0° to 45°C** | |

### 2.3.6 Applicability of NIMBUS 7 to OTEC Resource Assessment and Monitoring

The described sensors potentially offer oceanographers a unique data set. The advent of microwave imagery will allow more exact sea surface temperature and sea state analysis, without the hinderance of cloud cover, but at reduced spatial resolution. The CZCS provides an alternative means of water mass identification, in addition to the synoptic study of particulate and dissolved substances. To this end, one of the specific goals of the NIMBUS 7 program is to establish a number of data use demonstrations. These demonstrations will develop techniques useful for daily monitoring of an OTEC resource or facility.

Two specific uses of the CZCS for OTEC resource monitoring are: (1) Site specific variability of ocean color which may be associated with variability of phytoplankton before and during OTEC plant operations; and (2) Ocean front detection and analysis which will be useful in estimating the variability of the thermal resource at depth when summer insolation destroys the surface thermal signatures. In situ studies of the optical properties of the water will provide fundamental data for the quantitative interpretation of CZCS observations. The effect of artificial OTEC plant upwelling on the near surface phytoplankton populations may be quantified through such site specific studies and then extended to other areas of the ocean where OTEC plants are being considered. The tropical oceans are well suited for OTEC plants, and there is where the CZCS should contribute most effectively.

The SMMR on NIMBUS-7 is identical to the instrument on SEASAT, but with the failure of SEASAT, this instrument provides the primary source of surface roughness information and surface temperatures in cloudy regions. Although wind direction information is not available from the SMMR, standard meteorological analyses can provide good directional information such that, potentially, 25 km resolution speeds and direction can be obtained daily in certain select areas. Information on speed variability is of fundamental importance to OTEC plant operations and its operating environment.

## 2.4 GOES 1, 2, 3

### 2.4.1 Introduction

In 1974 NASA launched its first Synchronous Meteorological Satellite (SMS 1) as the first spacecraft in NOAA's Geostationary Operational Environmental Satellite (GOES) program. The second (SMS 2) was launched in 1975. These were followed by NOAA's operational GOES 1 and GOES 2. GOES 3 is almost identical to the four earlier satellites, and was launched in June, 1978. It assumed a circular earth-synchronous orbit at 35,800 km. At present, GOES 3 monitors much of the Pacific Ocean and the western half of the United States. GOES 2 is over South America, and GOES 1 was recently moved to a position over the Indian Ocean. Three more geostationary spacecraft are planned during the next eight years.

The objectives of the GOES program are: (1) to provide high resolution visual and infrared imaging over large areas of North and South America and the surrounding oceans every 30 minutes (see Figure 4), (2) to provide data collection from remote observing platforms, (3) to measure energetic particle flux and X-rays from the sun, also the strength of the earth's magnetic field, and (4) to broadcast centrally prepared weather and satellite information.

## 2.4.2 Instruments

The instrument payload on board GOES 3 includes: (1) Visible-Infrared Spin-Scan Radiometer (VISSR), (2) meteorological Data Collection and transmission System (DCS), (3) Energetic Particle Monitor (EPM), (4) Solar X-ray Monitor, and (5) Magnetic Field Monitor. The DCS and VISSR systems may be utilized in an OTEC resource or facility monitoring program. These will be discussed in detail.

## 2.4.3 Visible-Infrared Spin-Scan Radiometer

The VISSR provides measurements of the earth in the 0.55-0.75 μm (visible) band during daylight and in the 10.5-12.5 μm (infrared) band both day and night. VISSR images of the global disk are generated by the progressive stepping of a scan mirror and the 100 RPM rotation of the spacecraft. Approximately 18 minutes are required to scan the earth from northern to southern polar regions. The resulting visible image has a resolution of about 1 km, the infrared image has a resolution of 9.3 km. In addition to the normal scan mode, the radiometer may be placed in a limited scan mode. This reduces the area of coverage, but increases the frequency of imaging. In the normal mode, GOES 3 will produce 17,520 full disc images per year.

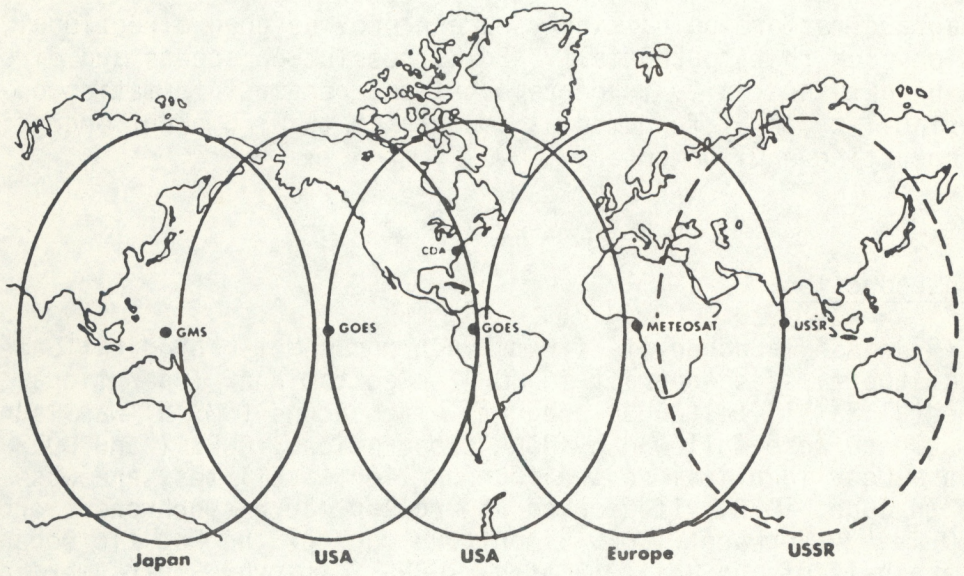


*Figure 4. Anticipated world-wide coverage of the geostationary satellite system when all five vehicles are in orbit. Specifications for GMS and METEOSAT differ only slightly from GOES.*

### 2.4.4 Data Collection System

With the advent of GOES, a satellite environmental data collection capability became a reality. The DCS has the following capabilities: (1) collects and distributes environmental data measured on remotely located data collection platforms (DCP), (2) collects all data on a scheduled or request basis, and (3) collects data from a minimum of 10,000 DCP's in a six-hour period.

### 2.4.5 Applicability of GOES to OTEC Resource Assessment or Monitoring Programs

The relatively low spatial resolution of the VISSR is compensated for by the extremely good temporal resolution. The production of 48 infrared images per day greatly increases the probability of a cloud free image. Recent reports show that GOES can obtain a view of the current boundary marking the continental edge of the Gulf Stream about two to three days out of five. Spectral analysis of the movements of the Stream's continental edge suggest that the lowest frequency is of the order of five days, which allows some degree of predictability over short time scales. Exploitation of these preliminary results is of value to OTEC thermal resources assessment and operations: The ocean surface monitoring capability of GOES during plant operation is most useful for determining the onset of large surface water temperature changes, and least for detailed study of the effect of the plant on the environment, because of the low spatial resolution.

The DCS, when used with the appropriate instrumentation, provides the capability of obtaining subsurface data in a real-time mode. This system may prove useful in the assessment of remotely located potential OTEC sites. In addition, each plant can be considered an automatic surface weather reporting platform, and the DCS used to monitor environmental conditions. The DCS may also prove useful for transmitting engineering data on the plant operations for a central monitoring facility.

## 2.5 GEOS-3

### 2.5.1 Introduction

The Geodynamics Observing Satellite series was initiated by NASA to provide data that could be interpreted for geophysical purposes such as the determination of the earth's gravity field variations, and the determination of the marine geoid. GEOS-3, the third in this series, was launched in 1975 and carried a precision altimeter into space which would provide the first long-term measurements of sea surface topography. The goal is to map sea surface topography to an absolute accuracy of 5 m with a relative precision of 1 meter, and to determine surface wave heights along the suborbital track. Sea surface topography can be used to determine surface geostrophic currents normal to the suborbital track if sufficient precision can be obtained in the measurements of the altimeter and the tracking systems.

GEOS-3 is in a low altitude (900 km) geocentric orbit, which has an incliniation of 115° and a period of 103.5 minutes. The spacecraft has been operating successfully since its launch and has exceeded all design criteria for accuracy and precision of the altimeter subsystem.

### 2.5.2 Instruments

The primary instrument aboard the GEOS-3 spacecraft of interest to OTEC is the altimeter, which is described in detail in the next section. A c-band transponder subsystem aboard GEOS-3 is used for range, range-rate, and angle measurements to track the spacecraft. A laser cube reflector system is used for ground based precision tracking. The doppler techniques of timing and measuring the frequency shift of radio transmission from a moving spacecraft is used to further establish the structure of the earth's gravitational field. High quality tracking information is critical to the oceanographic application of GEOS-3 data because sea surface topography measurements hinge equally on tracking and altimeter accuracy.

### 2.5.3 Radar Altimeter System

The altimeter is designed to accurately measure the distance from the spacecraft to the ocean's surface along the nadir track. To meet the objectives of the experiment, the altimeter has two distinct gathering modes: a long-pulse mode and a short pulse mode. Both modes operate on a 13.9 GHz frequency, both use a parabolic antenna, both have a maximum range acquisition time of six seconds and both have an altitude gravilarity of ± 0.2 meters. Differing characteristics are: (1) altitude data rate for the long pulse is two readings per second and six readings per second for the short pulse; (2) input power for the long pulse is 50 watts and for the short pulse it is 150 watts. The GEOS-3 radar altimeter has several features in common with the radar altimeter used on the SKYLAB satellite, but has the advantages of improved accuracy and the ability to operate over extended areas for greater periods of time, thereby providing the capability to examine the earth over longer arcs and observe extensive ocean areas.

### 2.5.4 Application to OTEC Resource Assessment and Monitoring

Data from the GEOS-3 satellite altimeter will probably not be available for much longer since the spacecraft has already outlived its design life time by a factor of 3 or so. The data can provide an invaluable source of information on ocean current strength variability, particularly in an enclosed sea such as the Gulf of Mexico. The geostrophic equation,

$$fv = g\frac{\partial h}{\partial x}$$

which describes the surface velocity v normal to the x coordinate is dependent on the Coriolis parameter f, the gravity field g, and the

surface height h gradient $\partial h/\partial x$. It is necessary to measure $\partial h/\partial x$ along an equipotential surface, the geoid, in order to obtain absolute values of the component of surface current speed normal to the sub-satellite track. It is unnecessary to know the geoid to the same accuracy required of $\partial h/\partial x$ if absolute values are unnecessary and variability only is of value. For the OTEC application in the Gulf of Mexico, maps of mean sea surface topography relative to the fixed (coastline) baseline and maps of variance about that mean, give important information on regions of current energetics. Regions of low variance would be potential OTEC plant sites if the thermal resource were also adequate. Subtracting the mean dynamic topography from the mean sea surface topography yields the local marine geoid. If successful, the geoid could be used to determine $\partial h/\partial x$ and the absolute current speeds, current direction could be determined at certain times of the year from the infrared satellite data coupled with shipboard surface truth measurements.

## 3.0 EXAMPLES OF SATELLITE DATA AND POTENTIAL OTEC USES

In this section, examples are given of the output products from the several satellites and sensors discussed in Section 2. Some of the data are being considered in their historical sense for the potential knowledge about oceanic variability that may be gleaned from them. Other data are considered as to the future potential for application to OTEC plant operations and monitoring requests. Some data fall into both categories. Altimetry data (Section 3.5) is most usefully thought of in its historical sense because the GEOS-3 has been operating well beyond its design lifetime. Data for future potential are the synthetic aperature radar data (Section 3.3), the coastal zone color scanner data (Section 3.4), and the scanning multifrequency microwave radiometer (Section 3.6). Data that can be considered useful for both its historical value and for its future contributions are the polar orbiting very high resolution radiometer data (Section 3.1), the visible-infrared spin-scan radiometer data from the geostationary operational environmental satellite (Section 3.2), and the buoy trajectory data (Section 3.7) from TIROS-N.

### 3.1 AVHRR Imagery

The advanced very high resolution radiometer aboard TIROS-N is designed to observe the entire earth twice a day. The spacecraft is in a 870 km high orbit, which is almost half that of the earlier NOAA series of spacecraft with their very high resolution radiometer (VHRR). Due to the lower orbit, the useful swath width on the AVHRR is less than on the older VHRR. Figure 5 depicts two of the AVHRR channels (0.550.68 μm visible and 10.5-11.5 μm infrared) over the eastern United States. AVHRR also has a 3.55-3.93 μm infrared channel which when used at night simultaneously with the 10.5-11.5 μm channel, can correct cloud-free scan spots for infrared atmospheric effects. This capability will eventually allow direct sea surface temperature measurements to less

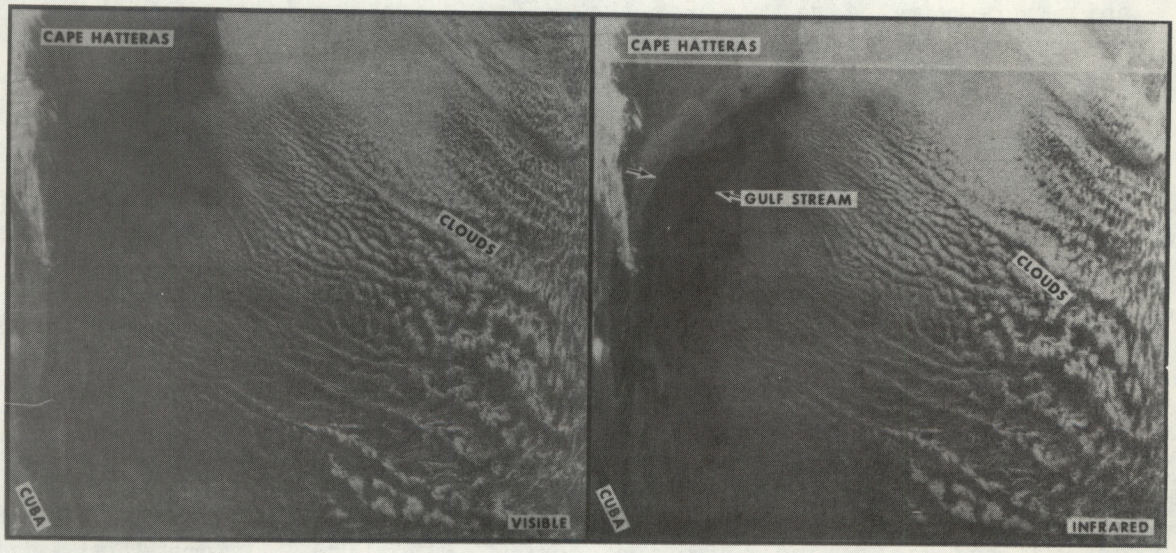


*Figure 5. AVHRR image of the Gulf Stream off the southeast coast of the United States. Left panel is reflected visible data from band 1 (0.55-0.68 μm); right panel is emitted infrared data from band 4 (10.5-11.5 μm). The stripe through the infrared image near Cape Hatteras is a data processing fault not associated with the Sensor. Subsync-lines are at ± 55° nadir angle and the distance across the image is approximately 2500 km. Note the extreme fore shortening near the limbs which is due to the low (870 km) altitude of TIROS-N (E. P. McClain, personal communication.*

than 1°K accuracy. The AVHRR as presently configured, can only make the direct sea surface temperature estimates at night because reflection in the 3.55-3.93 μm channel seriously affects the measured surface radiance. Night-time measurements suffer from uselessness of the visible channel for cloud detection which increases the uncertainty of sea surface temperature determination from the AVHRR. The spatial resolution of the AVHRR is 1.1 km at nadir which is 20% coarser than the VHRR which it supersedes. In some respects, the AVHRR is not an advance for oceanic observations over earlier systems, and in some cases it is less useful, particularly with respect to areal coverage. For OTEC applications, the AVHRR will provide the highest resolution imagery from a civilian spacecraft which will have value in observing the thermal effects of a plant in some detail, and for observing small sized thermal features (such as eddies) as they interact with the surrounding surface thermal resource.

## 3.2 VISSR Imagery

Figure 6 is a GOES infrared image obtained by the VISSR for the eastern Gulf of Mexico and the southeast coast regions of the United States. The major feature distinguishable in the eastern Gulf of Mexico is the Loop Current, which appears as a dark (warm) region in the image. The Loop Current is partially obscured by clouds in the southwestern portion. These data will be very useful for determining relative temperature variations associated with major currents, such as the Loop Current, and with ocean thermal perturbations which may affect the OTEC thermal resource. The data frequency (an image once every half hour) may provide more cloud free imagery since imagery may be acquired in cases of momentary breaks in cloudiness more often than by orbiting satellites. Therefore, these data will enhance the ability to detect thermal perturbations which may affect the OTEC resource. However, since the ground resolution of the VISSR is about 9 km and that for the AVHRR is 1 km, the VISSR data wil not yield as detailed an analysis of the sea-surface temperature structure as the AVHRR data. Therefore, small scale perturbations observed in the VISSR data should be verified by AVHRR data whenever possible.

## 3.3 SAR Imagery

The synthetic aperature radar images a 100 km wide swath along the suborbital path of the SEASAT using a 1.35 $GH_z$ microwave transceiver. Energy scattered back to the spacecraft is Bragg scattered from 11 cm wavelength ocean surface gravity waves. The motion of the spacecraft is used to synthesize a large antenna which reduces the resolution cell to 25 m, thus permitting high resolution imagery through clouds of ocean surface waves and other such features. Figure 7 is an example of SAR imagery from SEASAT taken in July 1978 over the Florida Current near Palm Beach, Florida. Interpretation of the image is speculative because there is little concurrent surface information available. The cellular features on the bottom left and center of Figure 7 are probably related to cumulonimbus activity in the Straits of Florida; the weather radar at Palm Beach

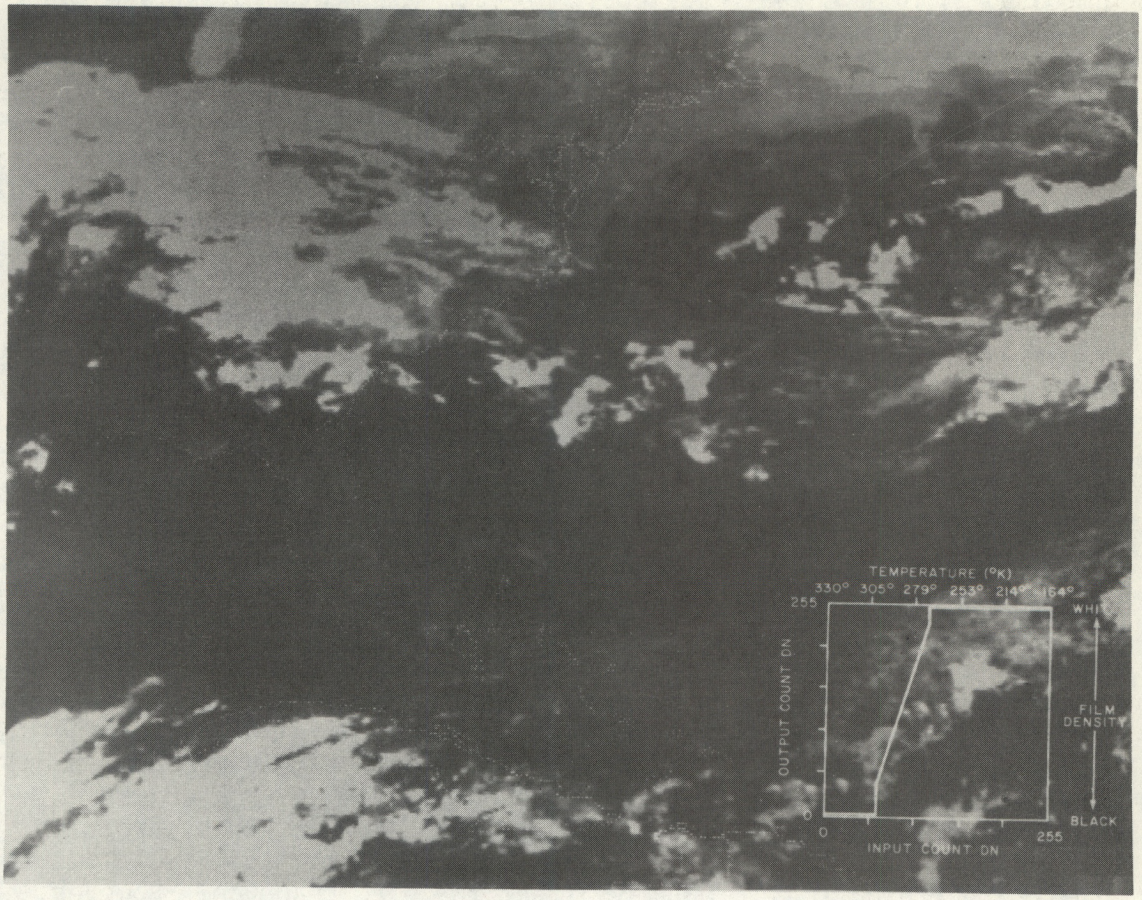


*Figure 6. VISSR infrared (10.5-12.5 μm) image of the east coast of the United States and eastern Gulf of Mexico. Spatial resolution is approximately 10 km, or an order of magnitude less than the AVHRR image shown in Figure 3.1. Gulf Stream rings and eddies are easily seen south of New England, and the Gulf Loop Current is seen in the original image in the eastern Gulf of Mexico. Images such as shown here have been acquired once each hour with the enhancement curve shown on the lower right since May 1, 1977 (from Maul, et al. 1978).*

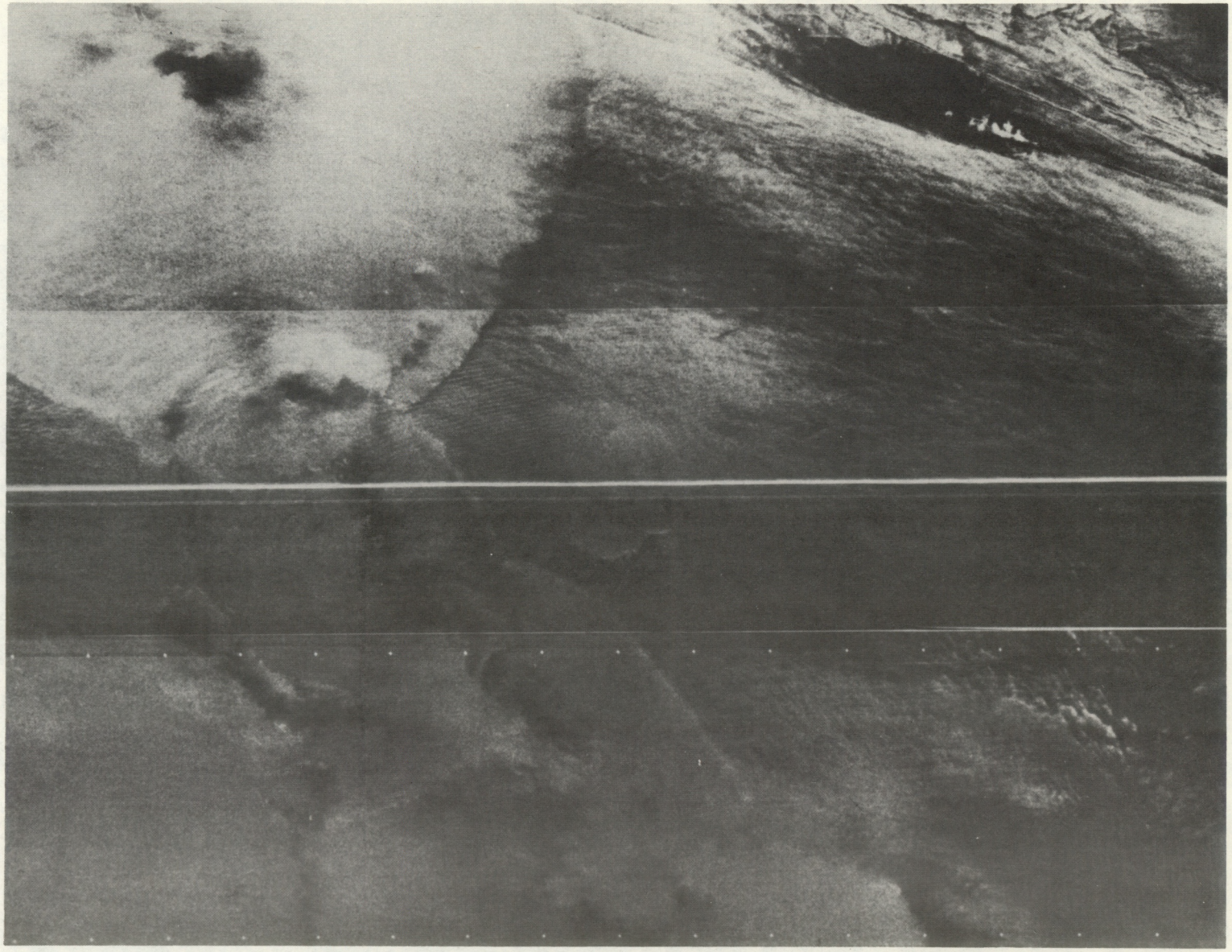

*Figure 7. SAR image from SEASAT-A of an area of the sea northeast of Palm Beach, Florida, centered at 27.7°N, 79.5°W. SAR images are processed in 25 km wide strips; area shown above is approximately 100 km x 130 km. Feature identification is unresolved at this writing; see text for details (D. Ross, personal communication).*

showed several storms of the size suggested in the SAR image at the same location. Just above the cell-like features in the left center of Figure 7 are wave-like patterns, probably caused by swell. From known relationships, periods can be calculated, and reasonable (empirical) estimates made of sea state. In the upper right-hand corner of Figure 7, a series of elongated ribbons can be seen. These may be the typical slicks associated with the edge of the Gulf Stream and, if so, are the radar analog of the usual visual manifestations (cf. Maul, 1978). Alternately, these patterns could be surface expressions of internal wave activity (cf. Elachi and Apel, 1976), which may or may not be associated with the edge of a current.

The synthetic aperature radar is in its very early stages of application to oceanography, and the ultimate value to OTEC cannot be stated at this time. Potentially, however, any 25 m resolution all weather observation of the sea could form a major component of a monitoring system for OTEC application.

## 3.4 CZCS Imagery

An example of computer processed imagery from the coastal zone color scanner over the eastern Gulf of Mexico is shown in Figure 8. The original image is a false color rendering of three CZCS channels, processed on the General Electric Image 100 System. The Image 100 used could not store all the data for a full resolution rendering of the original CZCS scene, so the data in Figure 8 are at 1.6 km spatial resolution; original CZCS data are at 0.8 km resolution at nadir. Figure 8 is from data acquired in November 1978, and shows a band of clouds stretching NW-SE across the lower left-hand quadrant of the image. To the west of the Mississippi River Delta an "S" shaped smoke plume is visible. Sediments in the water can be seen near the delta, off Mobile Bay, of Cape San Blas, off Tampa Bay, and in Florida Bay north of the keys. Algorithms are being developed for CZCS data which are intended to provide images of suspended sediment concentration and chlorophyll concentration. It would be imprudent to further interpret Figure 8 without surface truth measurements. One other CZCS image is available for analysis at this writing and it appears to show some remarkable details of the circulation in Florida Bay which is in qualitative agreement with current meter studies conducted at an earlier date. At Gulf of Mexico latitudes, the CZCS will acquire data about every two days at local noon. Therefore, only lower frequency phenomena (period $\geq$ four days) can be studied. On the other hand, the spatial resolution allows short wavelength ($\lambda \geq 1.6$ km) variability to be studied, and this seems to be directly applicable to investigations of the impact of OTEC plants on the environment.

## 3.5 Altimetry Data

Figure 9 is an example of the altimetric data obtained from GEOS-3 across the Gulf Stream (see the inset in the figure) off the South Carolina coast. The upper profile is the raw radar altimeter data (in meters), the middle profile, the smoothed altimeter data, and the lower

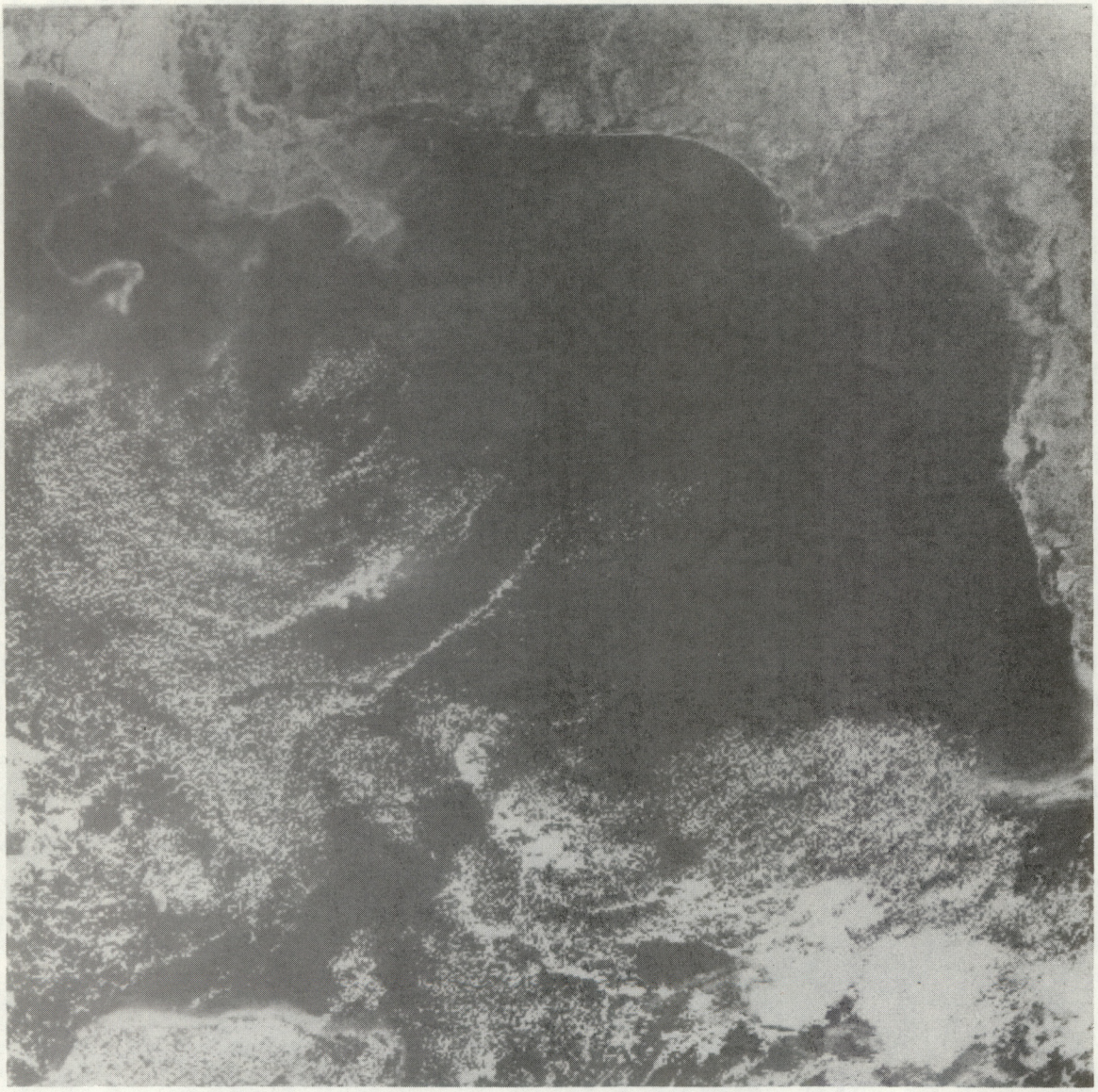

*Figure 8. CZCS image of the northeastern Gulf of Mexico processed from three channels of bandpassed data (cf. Figure 2). Resolution of the original image has been degraded so that the individual picture elements (pixels) appear as squares. Original image was a false color print with the land in shades of yellow, the shallow water in shades of green, and the deep water in shades of brown (J. Mueller, personal communication).*

profile is the output of the automatic gain control (AGC), a function of the ocean backscatter. The time scale was arbitrarily set so that a 250 second time mark corresponded to a position just inland of the South Carolina coast. The position of the Gulf Stream estimated from the altimetry data corresponded well with the mean position of the Gulf Stream in the inset.

Current data are an important environmental parameter for OTEC. These data will be useful in siting OTEC in regions where currents will not produce mooring problems. They will also be used to determine the transport and diffusion of the water-mass discharged by OTEC. The altimetry data can be used to detect intense current systems, and can possibly be used to estimate the magnitude of current. However, present altimetry systems are "nadir looking" so that integration of orbital data will be required in order to obtain spatial analyses. Such analyses will only be useful in current systems which vary slowly in time, generally major current systems such as the Loop Current. Single profiles such as that in Figure 9 would have value in smaller scale perturbations which vary appreciably in time. However, analysis of variance of large amounts (years) of altimetry data may define in a given region locations of large energy as large variations in energy. This information would have value in siting OTEC.

## 3.6 SMMR Wind Data

The surface stress, or surface winds, is one of the major forcing functions influencing the behavior of the ocean. Sparsity of wind data over the oceans has precluded detailed analyses on a time and space scale commensurate with some of the higher frequency, small scale oceanic phenomena. Large-scale wind analyses over the ocean have been performed using averaged data obtained by integrating data from ships of opportunity.

However, with the launch of NIMBUS 7, the possibility exists to obtain spatial analyses of wind speed in a given region every six days. In some regions, the period may be shorter than six days due to overlapping. Figure 10 shows the relationship between wind speeds obtained by the SMMR (in this case the SMMR was on SEASAT which launched before NIMBUS 7, and the instrument is the same as that aboard NIMBUS 7) and *in situ* wind speeds obtained from ships of opportunity. The data were collected in the Gulf of Alaska on 23 September 1978. The analysis indicate a very good correlation between the SMMR wind speeds and the observed wind speeds.

The potential for obtaining wind speed analysis on a high temporal and spatial resolution leads to the potential for analysis and publication of the influence of the wind on the ocean and for analysis of sea-state, in terms of both average and existing conditions. The former is important with respect to understanding the influence of the winds on perturbations and the generation of perturbations which may influence OTEC operations. The latter is important with respect to siting an OTEC in a given region.

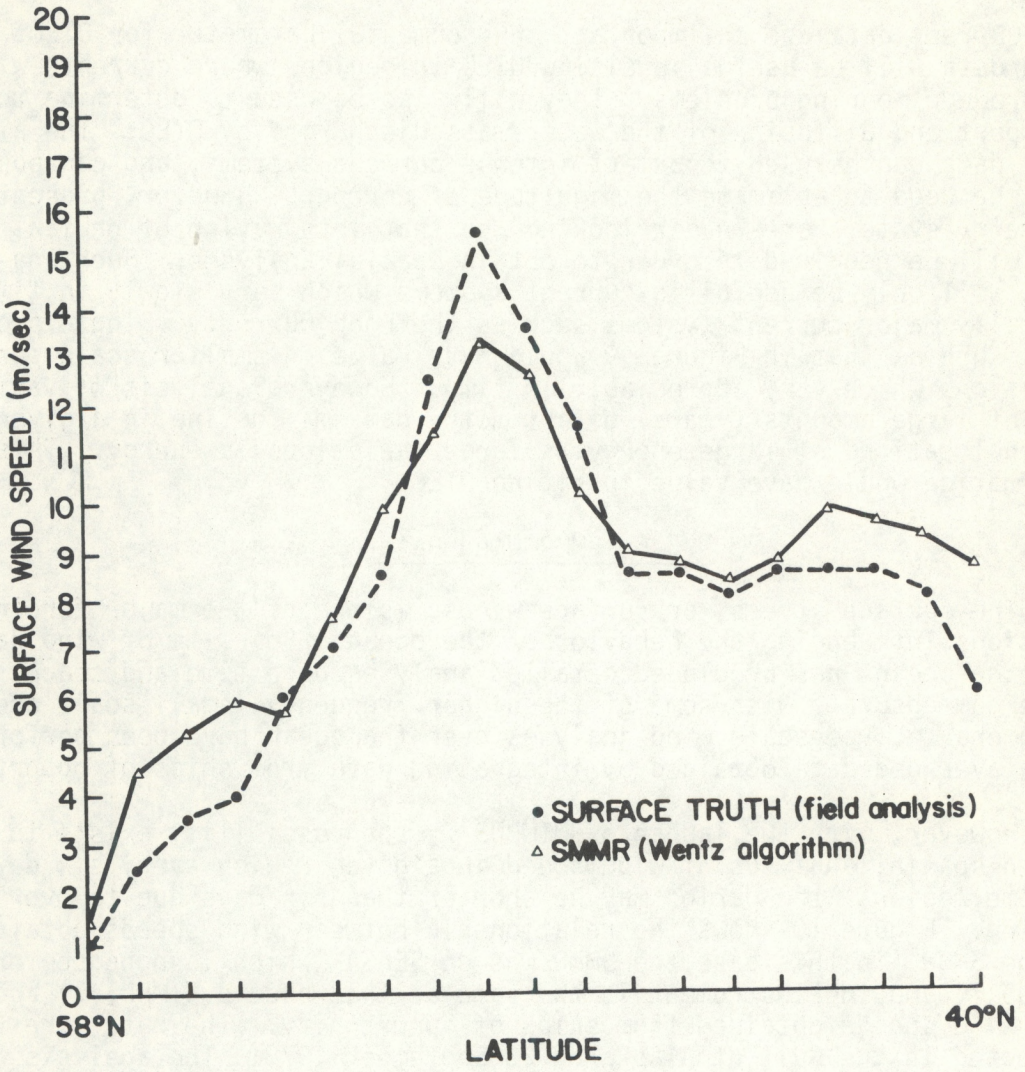


*Figure 10. Preliminary result from analysis of SEASAT-A scanning multifrequency microwave radiometer data for surface wind speeds in the Gulf of Alaska. Surface truth (dots) is from the field analysis closest in time to the satellite overpass. SMMR data are available from the NIMBUS 7 spacecraft but no operational system is functioning (D. Ross, personal communication).*

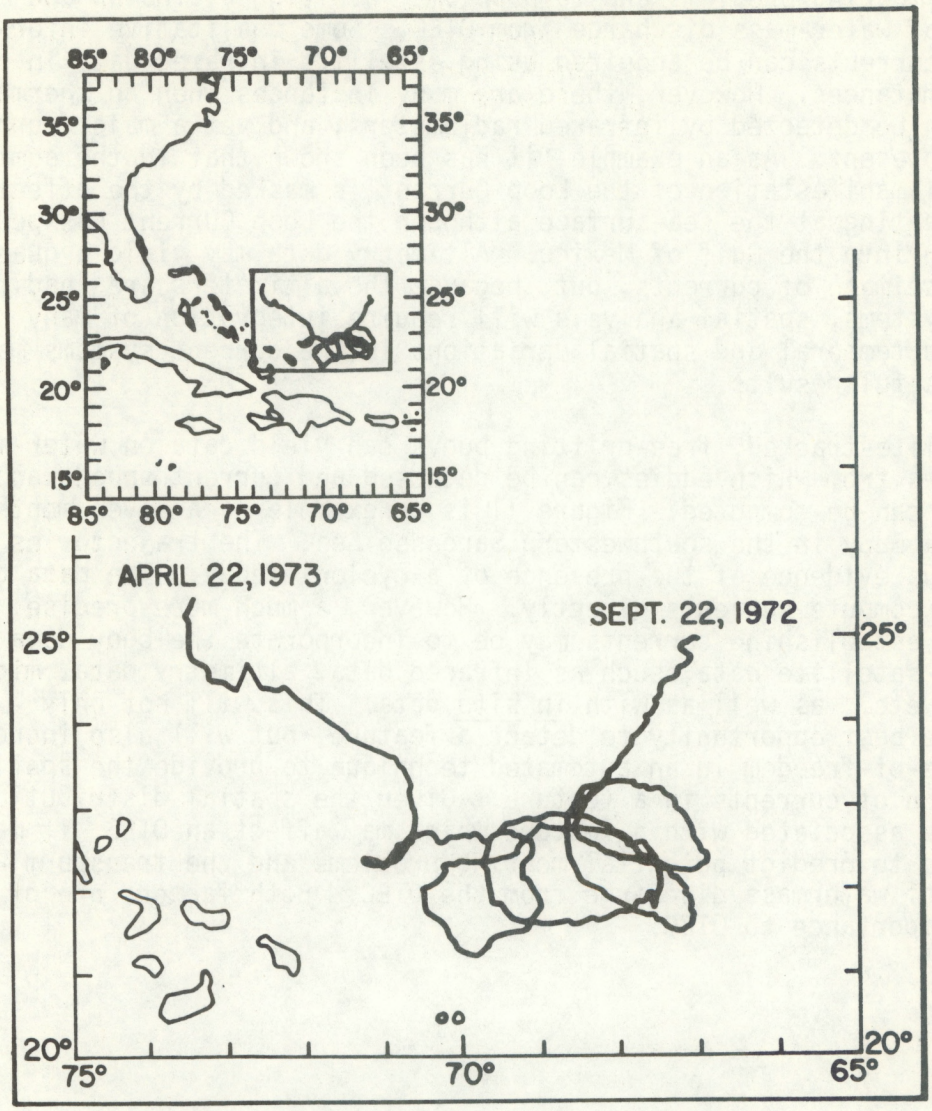


*Figure 11. Example of a free drifting surface buoy track in the subtropical western North Atlantic Ocean. Buoy was located by a satellite doppler location system approximately twice a day. Region shown was thought to be dominated by the Antilles Current, but now is seen to be influenced by eddy-like circulations.*

## 3.7 Buoy Trajectories

An important environmental parameter required by OTEC is knowledge of current speeds and directions. Such information is required with respect to mooring problems and to problems involving diffusion and transport of water-mass discharge from OTEC. Some qualitative information on currents can be acquired using satellite infrared data in certain circumstances. However, there are many instances when no thermal feature can be detected by infrared radiometers, and yet a major current system is present. As an example, it has been shown that in the summer, the thermal manifestation of the Loop Current is masked by the effects of solar heating at the sea-surface although the Loop Current has penetrated deep into the Gulf of Mexico. Altimetry data may yield a quantitative estimate of currents, but, because the altimeters are "nadir looking" systems, spatial analysis will require integration of many orbits, and temporal and spatial variations in the current systems may prohibit useful results.

Satellite-tracked, free-drifting buoys can yield data on water-mass trajectories from which eddies can be detected and current speeds and directions can be computed. Figure 11 is an example of a seven month record of a buoy in the southwestern Sargasso Sea. The trajectories show obvious evidence of the presence of a cyclonic eddy. The data can be used to compute currents directly. However, a much more precise method for establishing currents may be to incorporate the buoy data with other satellite data, such as infrared data, altimetry data, microwave data, etc., as well as with *in situ* data. This will not only provide the best opportunity to detect a feature, but will also increase the degrees-of-freedom in an automated technique to provide the spatial distribution of currents in a feature. Given the spatial distribution of currents associated with a feature which may affect an OTEC, it may be possible to predict potential mooring problems and the transport and diffusion of watermass discharge from the OTEC. Both factors are of critical importance to OTEC.

Table 10: Satellite Sensors and Data Characteristics

| Instrument | Spacecraft | Spectral Bands | Nominal Resolution | Swath Width | Repeat Coverage | Applications |
|---|---|---|---|---|---|---|
| Altimeter | GEOS-3<br>SEASAT-A | 2.1 cm<br>2.2 cm | 3.6-14.3 km<br>1.6 km | < 25 km<br>< 12 km | 37 days<br>* | Global coverage of sea surface topography with accuracy of < 5 m and precision < 1 m (better on SEASAT). |
| Advanced Very High Resolution Radiometer | TIROS-N | 0.55-0.68 μm<br>0.72-1.10 μm<br>3.55-3.93 μm<br>10.5-11.5 μm | 1 km for HRPT<br>4 km for GAC | 2800 km | 12 hours | Global coverage of sea surface temperature with accuracy better than 15°K and precision better than 0.5°K, also global coverage of cloud cover and visible albedo. |
| Coastal Zone Color Scanner | NIMBUS 7 | 0.433-0.453 μm<br>0.510-0.530 μm<br>0.540-0.560 μm<br>0.660-0.680 μm<br>0.70-0.80 μm<br>10.5-12.5 μm | 825 m | 1600 km | 24 hours at > 50° latitude to 72 hours at 0° latitude | Global coverage of visible radiance, potentially analyzable as chlorophyll, gelbstoff, and temperature variability. |
| Defense Meteorological Satellite Program | DMSP | 0.55-1.0 μm<br>8.0-13.0 μm | 500 m or 4 km | 3000 km | 12 hours | Global coverage of temperature gradients with 1.6°K resolution, but not quantitative due to broad band of IR sensor. |
| Heat Capacity Mapping Mission Radiometer | AEM-1 | 0.5-1.1 μm<br>10.5-12.5 μm | 680 m | 700 km | 12 hour intervals every five days | High spatial resolution, <0.5°K NEΔT at 280°K for thermal inertia; local coverage only. |
| Multispectral Scanner | LANDSAT 1, 2 and 3 | 0.5-0.6 μm<br>0.6-0.7 μm<br>0.7-0.8 μm<br>0.8-1.1 μm | 80 m | 185 km | 18 days (nine days between two spacecraft) | Highest spatial resolution visible data with very limited coverage away from CDA stations; sensitive to chlorophyll and suspended sediments. IR channel on LANDSAT-3 failed early in mission. |
| Synthetic Aperature Radar | SEASAT-A | 23.5 cm | 25 m | 100 km | * | Limited data due to SEASAT failure; all weather surface wave and surface frontal information. |

*Failed October 1978

Table 10: Satellite Sensors and Data Characteristics (Continued)

| Instrument | Spacecraft | Spectral Bands | Nominal Resolution | Swath Width | Repeat Coverage | Applications |
|---|---|---|---|---|---|---|
| Scatterometer | SEASAT-A | 2 cm | 50 km | 500 km | * | Limited Data due to SEASAT failure; wind speed ($< 30\ m\ s^{-1}$) and direction ($\pm\ 20^{o}$), global coverage. |
| Scanning Multi-frequency Micro-wvve Radiometer | NIMBUS 7<br>SEASAT-A | 4.55 cm<br>2.81 cm<br>1.67 cm<br>1.36 cm<br>0.81 cm | 110 km<br>70 km<br>45 km<br>35 km<br>20 km | 900 km | six days | Global coverage of low resolution surface temperature $< 3^{o}K$ precision, $< 1.5^{o}K$ precision, and surface wind speed ($< 50\ m\ s^{-1}$); no wind direction. Identical instruments on SEASAT and NIMBUS. |
| Scanning Radiometer | NOAA 1-5 | 0.5-0.7 μm<br>10.5-12.5 μm | 8 km | 3000 km | 12 hours | Global coverage, high resolution temperature with accuracy better than $2^{o}K$ and precision better than $1^{o}K$. |
| Temperature Humidity Infrared Radiometer | NIMBUS 4-7 | 6.5-7.0 μm<br>10.5-12.5 μm | 20 km<br>7 km | 2600 km | 12 hours | Global coverage of moisture content of stratosphere and sea surface temperature with accuracy better than $2^{o}K$ and precision better than $0.5^{o}K$. |
| Very High Resolution Radiometer | NOAA 2-5 | 0.6-0.7 μm<br>10.5-12.5 μm | 1 km | 3000 km | 12 hours | Global coverage, high resolution temperature with accuracy better than $1.5^{o}K$ and precision better than $1^{o}K$. |
| Visible Infrared Radiometer | SEASAT-A | 0.5-0.9 μm<br>10.5-12.5 μm | 4 km | 1500 km | * | Limited data due to SEASAT failure |
| Visible Infrared Spin-Scan Radiometer | GOES 1-3 | 0.55-0.7 m<br>10.5-12.5 m | 1 km<br>8 km | Full Disk | 30 minutes | Global coverage high resolution temperature with accuracy better than $2^{o}K$ and precision better than $0.5^{o}K$. |

*Failed October 1978

# 4.0 SUMMARY

Satellite sensors which have the resolution, accuracy and repeat coverage that make them useful to OTEC considerations are summarized in Table 10. A number of satellite sensors are included in Table 10 that were not discussed in chapter 2. The sensors discussed in chapter 2 are the most useful for the OTEC program, or have significant potential (in the case of the SEASAT sensors). There are some limited applications of the DMSP, AEM, and LANDSAT sensors to OTEC monitoring needs and they were included in the table for completeness.

Sensors have to be part of several compromises which include the orbital characteristics of the spacecraft, the electrical power available, the telemetry subsystem, calibration requirements, etc. For these reasons, no single sensor is optimized for even the most fundamental variable: sea surface temperature. Probably the most useful spacecraft for quantitative measurement of sea surface temperature is the TIROS-N series and the follow on series, NOAA A-G. Probably the most ideal way of measuring mid to low latitude sea surface temperature would be from a geostationary vehicle with the proper sensor design; GOES 1-3 is marginally useful because of poor calibration design (again a compromise).

Data archiving is of major importance to the OTEC community if any analysis of historical records is to be attempted. In general, no VHHR are archived. GOES data are being archived at three hour increments from September 1978 onward; prior to this date, only one visual/infrared pair per day was saved from July 1976 onward. AVHRR data at 4 km resolution data are not. Almost all the data from experimental satellites (i.e., NIMBUS, AEM, SEASAT, LANDSAT, and GEOS) are archived, usually by NASA; archiving of the operational data is done by NOAA's EDIS.

It was emphasized throughout the report that remote sensing is not capable at this stage in its development to independently provide all the observations necessary for measurement of a given variable. That point is reiterated here in conclusion so that the over-zealous selling of satellite oceanography of the past is a mistake not repeated. Only an integrated in situ and remotely sensed measurement system can offer high quality data needed for environmental research.

## 5.0 REFERENCES


Apel, J. R. and J. W. Sherman, III (1973). Monitoring the seas from space: NOAA's requirements for oceanographic satellite data. A report to the NOAA Satellite Plans and Requirements Storing Group, NOAA, AOML-LORS 6.73.1, Miami, Florida, 38 pgs.

Bristor, C. L. (1975). Central processing and analysis of geostationary satellite data. NOAA Technical Memorandum, NESS 64, U.S. Department of Commerce. National Environmental Satellite Service, Washington, D.C.

Corbell, R., C. Callahan and W. Kotsch (1976). The GOES/SMS user's guide. *Management and Technical Services Company*, (Contract NAS 5-20694), National Aeronautics and Space Administration, Goddard Space Flight Center, Greenbelt, Maryland.

____ (1977). They've Got You Covered. *NOAA*, Vol. 7, No. 4, pp. 26-27.

____ (1978). Satellites Undergo Maneuvers. *NOAA*, Vol. 8, No. 4, p. 61.

Elachi, C. and J. R. Apel (1976). Internal wave observations made with an airborne synthetic aperature imaging radar. *Geophys. Res. Ltrs.*, 3(11), pp. 647-650.

Huston, W. B., L. Hardis, C. Horvath and H. Soule (1978). NIMBUS 7 data applications system data plan. *OAO Corporation* (Contract NAS 5-22420), National Aeronautics and Space Administration, Goddard Space Flight Center, Greenbelt, Maryland.

Madrid, C. R. (1978). The NIMBUS 7 user's guide. *Management and Technical Services Company* (Contract NAS 5-23740), National Aeronautics and Space Administration, Goddard Space Flight Center, Greenbelt, Maryland.

Maul, G. A. (1977). Recent progress in the remote sensing of ocean surface current. *Mar. Tech. Soc. Journal*, 11(1), pp. 5-13.

Maul, G. A. (1978). Locating and interpreting hand-held photographs over the ocean; a Gulf of Mexico example from the Apollo-Soyuz test project. *Remote Sensing of Environ.*, 7, pp. 249-263.

Maul, G. A., P. W. deWitt, A. Yanaway and S. R. Baig (1978). Geostationary satellite observations of Gulf Stream meanders: Infrared measurements and time series analysis. *J. Geophys. Res.*, 83(C12), pp. 6123-6135.

Nagler, R. G. and S. W. McCandless (1975). Operational Oceanographic satellites, NASA, Washington, D.C., 12 pgs.

NOAA program development plan for SEASAT-A, Research and Applications (1977). U.S. Department of Commerce, NOAA/NESS, Washington, D.C.

Schwalb, A. (1978). The TIROS-N/NOAA A-G satellite series. NOAA Tech. Memo - NESS 95, U.S. Department of Commerce, NOAA, Washington, D.C. 75 pgs.

Vukovich, F. M., B. W. Crissman, M. Bushnell, and W. J. King (1978). Sea surface temperature variability analysis of potential OTEC sites utilizing satellite data. Contractor's Report, DOE Contract EG-77-C-05-5444. Research Triangle Institute, Research Triangle Park, North Carolina 27709, 153 pgs.

Wolf, P., H. Levit, J. Shuekart, and W. Wolf (1977). OTEC thermal resource report for central Gulf of Mexico. Contractor's Report, DOE Contract EC-77-C-01-4028. Ocean Data Systems, Inc., Monterey, California.

# 6.0 GLOSSARY

AEM-n (Applications Explorer Mission). Small, special purpose, spacecraft designed to observe an area with 12 hours between observations to measure thermal inertia, every five days. Sun-synchronous, circular 620 km altitude orbit with data acquisition when in view of a CDA station only.

ALT (SEASAT Altimeter). Vertical looking 2.2 cm radar altimeter flown on the SEASAT-1 experimental satellite with nadir only resolution of 1.6-12 km, and a precision of ± 10 cm.

ARGOS. Data collection and location system on TIROS-N which was designed, built, and furnished by the Centre National d' Estudes Spatiales (CNES) of France.

AVHRR (Advanced Very High Resolution Radiometer). Four channel (0.55-0.68 μm, 0.72-1.10 μm, 3.55-3.93 μm, 10.5-11.5 μm) scanning radiometer flown on the TIROS-N (NOAA-6) operational satellite with nominal resolution at nadir of 1 km for limited area coverage and 4 km for global coverage, and with swath width of 2850 km.

CDA (Command and Data Acquisition). A surface radio transceiver station for sending commands to a spacecraft and receiving relayed or direct data from the satellite.

CZCS (Coastal Zone Color Scanner). Six channel (0.433-0.453 μm, 0.510-0.530 μm, 0.540-0.560 μm, 0.660-0.680 μm, 0.70-0.80 μm, 10.5-12.5 μm) scanning radiometer flown on the NIMBUS 7 experimental satellite with nominal resolution at nadir of 825 m, and with swath width of 1600 km.

DCP (Data Collection Platform). A fixed or free floating platform with transmitter or transceiver for broadcasting data to a satellite receiver for relay to a command and data acquisition station.

DCS (Data Collection System). 1) On TIROS, a random access system to acquire data from fixed and free-floating platforms with doppler platform location capability; 2) On GOES, an interrogate-receive system to acquire data from fixed and free-floating platforms with no doppler platform location capability; 3) On LANDSAT, a receive only system to acquire data from fixed platforms with no doppler platform location capability.

DMSP (Defense Meteorological Satellite Program). Operational series of sun-synchronous, polar orbiting, 850 km altitude, $99^{o}$ inclination, satellites with dual channel (0.55-1.0 μm, 8-13 μm), dual resolution (0.5 km, 4 km), scanning radiometers which have a swath width of 3000 km; minimum temperature resolution is 1.6 K at satellite.

EDIS (Environmental Data and Information Service). NOAA agency charged with the archiving of NOAA operational satellite data and all oceanographic data.

ERTS-n (Earth Resources Technology Satellite). Original name of the LANDSAT series of experimental land use spacecraft.

GEOS-n (Geodetic Earth-Orbiting Satellite). Experimental satellite series GEOS-3 had a precision radar altimeter (ALT) for sensing sea surface topography from 890 km altitude, in a non-sun-synchronous 115° inclination orbit.

GMS-n (Geostationary Meteorological Satellite). Japanese Space Agency's version of GOES-n, geostationary over equator near 135°E longitude.

GOES-n (Geostationary Operational Environmental Satellite). Operational series of geosynchronous satellites in equatorial orbit at 35,800 km altitude; longitude varies with specific satellite. Sensors aboard include the VISSR and DCS.

HCMM (Heat Capacity Mapping Mission). HCMM radiometer on AEM-1 spacecraft is a two band (0.5-1.1 μm; 10.5-12.5 μm) sensing radiometer with 600 m nominal resolution at nadir and a 700 km swath. Designed for thermal inertia studies.

HRPT (High Resolution Picture Transmission). Direct readout system for the AVHRR on TIROS-N; data from the TOVS is also available on the HRPT beacon.

ITOS-n (Improved TIROS Operational Satellite). ITOS D, E, F, and G are the pre-launch names of NOAA 2, 3, 4, and 5.

LANDSAT-n. Operational earth resources technology satellite series which are in geocentric 900 km altitude sun-synchronous 99° inclination orbits. Sensors onboard include the DCS, MSS, and RBV. Repeat coverage time is 18 days.

METEOSAT. European Space Agency's version of GOES-n, geostationary over equator near 10°E longitude.

MSS (Multispectral Scanner). Four channel (0.5-0.6 μm, 0.6-0.7 μm, 0.7-0.8 μm, 0.8-1.1 μm) scanning radiometer on the LANDSAT 1, 2 satellite (LANDSAT-3 had a fifth 10.5-12.5 μm channel) with nominal resolution of 80 m and swath width of 185 km.

NIMBUS-n. Experimental satellite series which carries new instruments for test and evaluation. NIMBUS 7 is in a 955 km sun-synchronous near-polar orbit and carries the CZCS, SMMR, and six other non-oceanographic instruments.

NOAA-n (National Oceanic and Atmospheric Administration). Series of five operational environmental satellites which were in a sun-synchronous, near polar orbit of 1450 km altitude at an inclination of 102°, equipped with an SR (NOAA 1-5), AVHRR (NOAA 2-5), and a VTPR (NOAA 4-5).

RAMS (Random Access Memory System). Fixed or floating platform location system onboard the NIMBUS 6 spacecraft which provides two position fixes per day with ± 5 km accuracy.

RBV (Return Beam Vidicon). Three camera system covering 0.47-0.575 μm, 0.58-0.68 μm, and 0.69-0.83 μm flown on the LANDSAT 1, 2 spacecraft with nominal ground resolution of 700 m in a viewed scene 185 x 185 km.

SAR (Synthetic Aperture Radar). Microwave (23.5 cm) imaging device flown on the SEASAT-1 experimental satellite with nominal resolution of 25 m and swath width of 100 km.

SASS (SEASAT Scatterometer System). Single wavelength (2 cm) active microwave scatterometer flown on the SEASAT-1 experimental satellite with nominal resolution of 50 km and with a swath width of approximately 500 km.

SEASAT-n. Experimental oceanographic satellite which is in a non-sun-synchronous circular orbit of 800 km at an inclination of 108°. Sensors onboard include the ALT, SAR, SASS, SMMR, and the VIR.

SMMR (Scanning Multifrequency Microwave Radiometer). Five wavelength (4.55 cm, 2.81 cm, 1.67 cm, 1.36 cm, 0.81 cm) passive microwave radiometer flown on SEASAT-1 and NIMBUS 7 with nominal resolutions of 110 km, 70 km, 45 km, 35 km and 20 km and a swath width of approximately 700 km.

SMS-n (Synchronous Meteorological Satellite). Prototype geosynchronous series in equatorial orbit at 35,800 km altitude. Identical to and forerunner of GOES-n series.

SR (Scanning Radiometer). Two channel (0.5-0.7 μm, 10.5-12.5 μm) scanning radiometer flown on the NOAA 1-5 series of operational satellites, with nominal resolution of 3.5 km in the visible channel and 8 km in the infrared, and with swath width of 3000 km.

THIR (Temperature/Humidity Infrared Radiometer). Two channel (6.5-7.0 μm, 10.5-12.5 μm) scanning radiometer flown on the NIMBUS 4-7 spacecraft with nominal resolution at nadir of 20 km and 7 km respectively and a 1300 km swath width.

TIROS-n. Third generation operational satellite which is in a sun-synchronous polar orbit, 870 km high. Sensors with oceanographic application include the AVHRR, DCS, and TOVS.

TOVS (TIROS Operational Vertical Sounder). A three instrument system consisting of a high resolution infrared radiation sounder, a stratospheric sounding unit, and a microwave sounding unit; permits calculation of atmospheric temperature and humidity profiles.

VHRR (Very High Resolution Radiometer). Two channel (0.6-0.7 μm, 10.5-12.5 μm) scanning radiometer flown on the NOAA 2-5 series of operational satellites, with nominal resolution at nadir of 1 km, mostly direct readout, and with swath width of 3000 km.

VIR (Visible/Infrared Radiometer). Two channel (0.5-0.9 μm, 10.5-12.5 μm) scanning radiometer flown on the SEASAT-1 experimental satellite with nominal resolution at nadir of 4 km, and with a swath width of 1500 km.

VISSR (Visible/Infrared Spin Scan Radiometer). Two channel (0.55-0.7 μm, 10.5-12.5 μm) scanning radiometer flown on the GOES series of geostationary satellites with nominal resolution of 1 km in the visible channel and 8 km in the infrared; and swath width of full earth disk.

VTPR (Vertical Temperature Profiling Radiometer). Multichannel vertical viewing radiometer used to determine atmospheric temperature profiles and total moisture, flown on NOAA 4 and 5.

# 7.0 SELECTED LITERATURE (1973-1978)


Abiodun, A. A. (1976). Satellite survey of particulate distribution patterns in Lake Kainji. Remote Sens. of Envir., 5, pp. 109-125.

Adiks, T. G., V. I. Dianove-Klokov, V. M. Ivanov and A. I. Semenov (1975). Continuum extinction in the 8-13 μm window under conditions of high atmospheric transparency. Atmos. Ocea. Phys., 11, 7, p. 431.

Almeida, S. P. and J. Kim-Tzong-Eu (1976). Water pollution monitoring using matched spatial filter. J. Applied Optics, 15, pp. 510-515.

Alpers, W. and K. Hasselmann (1978). The two-frequency microwave technique for measuring ocean-wave spectra from an airplane or satellite Bound. Layer Met., 13, pp. 215-231.

Anderle, R. J. and R. L. Hoskin (1977). Correlated errors in satellite altimetry geoids. Geophys. Res. Ltrs., 4, 10, pp. 421-423.

Anderson, A. C. (1978). Remote sensing in sea search and rescue. Remote Sens. of Envir., 7, pp. 265-273.

Anding, D. and R. Kauth (1970). Estimation of sea surface temperature from space. Remote Sens of Envir., 1, pp. 217-221.

Anding, D. and R. Kauth (1972). Reply to comment by G. A. Maul and M. Sidran. Remote Sens. of Envir., 2, pp. 171-175.

Andreyev, S. D., L. S. Ivlev and A. V. Poberovskiy (1974). Aerosol attenuation of radiation in the 8-13 μm atmospheric window. Atmos. Ocea. Phys., 10, 10, p. 682.

Antyufeyev, V. S. and M. A. Nazaraliyev (1973). A new modification of the Monte Carlo method for solution of problems in the theory of light scattering in a spherical atmosphere. Atmos. Ocea Phys., 9, 8, p. 463.

Apel, J. R., J. R. Proni, H. M. Byrne and R. L. Sellers (1975). Near simultaneous observations of intermittent internal waves on the Continental Shelf from ship and spacecraft. Geophys. Res. Ltrs., 2, 4, pp. 128.

Apel, J. R. et al. (1975). Observations of oceanic internal and surface waves from the earth resources technology satellite. J. Geophys. Res., 80, 6, pp. 865-871.

Apel, J. R. (1976). Ocean science from space. EOS Trans. AGU, 57, 9, pp. 612-624.

Apel, J. R., H. M. Byrne, J. R. Proni and R. Sellers (1976). A study of oceanic internal waves using satellite imagery and ship data. Remote Sens. of Envir., 5, pp. 125-137.

Baig, S. R. (1975). Comments on "Application of synchronous meteorological satellite data to the study of time dependent sea surface temperature changes along the boundary of the Gulf Stream," by R. Legeckis. Geophys. Res. Ltrs., p. 231.

Barrick, D. E. (1977). The ocean waveheight nondirectional spectrum from inversion of the HF sea-echo Doppler spectrum. Remote Sens. of Envir., 6, pp. 201-229.

Barrick, D. E. (1978). HF radio oceanography - a review. Bound. Layer Met., 13, 2, pp. 23-45.

Basharinov, A. Ye, A. K. Gorodetskiy,, A. S. Gurvich, S. T. Yegorov, A. A. Kurskaya, D. T. Matveyev, A. P. Orlov and A. M. Shutko (1973). Radiation temperatures of ground cover in the microwave and infrared ranges measured from the COSMOS-384 satellite. Atmos. Ocea. Phys., 9, 2, p. 99.

Blankenship, J. R. and R. C. Savage (1974). Electro-optical processing of DAPP meteorological satellite data. Bull. A.M.S., 55, 1, pp. 9-15.

Bliamptis, E. E. (1970). Nomogram relating true and apparent radiometric temperatures of graybodies in the presence of an atmosphere. Remote Sens. of Envir., 1, pp. 93-95.

Brandli, H. W., D. Reinke and L. E. Irvine (1977). Sea surface emission temperatures from defense meteorological satellite. J. Phys. Oceanogr., 7, 2, pp. 302-304.

Briscoe, M. G., O. M. Johannessen and S. Vincenzi (1974). The Maltese oceanic front: A surface description by ship and aircraft. DSR, 21, pp. 247-262.

Bristor, C. L. and W. L. Raynore (1977). Digital satellite imagery in industrial meteorology. Bull. A.M.S., 58, 6, pp. 480-487.

Brown, W. E., C. Elachi and T. W. Thompson (1976). Radar imagery of ocean surface patterns. J. Geophys Res., 81, 15, pp. 2657-2667.

Bugaev, V. A. (1973). Dynamic climatology in the light of satellite information. Bull. A.M.S., 54, 5, pp. 394-418.

Byalko, A. V. (1975). Relation of the statistical characteristics of reflected and refracted light to the surface-wave spectrum. Atmos. Ocea. Phys., 11, 6, p. 407.

Byutner, E. K. (1974). Interaction of a turbulent flow with a surface covered with moving obstacles. Atmos. Ocea Phys., 10, 7, p. 486.

Campbell, W. J. et al. (1976). Beaufort Sea ice zones as delineated by microwave imagery. J. Geophys. Res., 81, 6, pp. 1103-1110.

Campbell, W. J. et al. (1978). Microwave remote sensing of sea ice in the AIDJEX main experiment. Bound. Layer Met., 13, pp. 309-339.

Carpenter, D. J. and H. R. Jitts (1973). A remote operating submarine irradiance meter. DSR, 20, pp. 859-866.

Chau, H. L. and A. K. Fung (1977). A theory of sea scatter at large incident angles. J. Geophys. Res., 82, 24, p. 3439.

Coulson, K. L. (1974). Light polarization as an indicator of atmospheric optical properties. Atmos. Ocea. Phys., 10, 3, p. 143.

Cox, S. K. (1976). Observations of cloud infrared effective emissivity. JAS, 33, pp. 287-289.

Cram, R. and K. Hanson (1974). The detection by ERTS 1 of wind-induced ocean surface features in the lee of the Antilles Island. J. Phys. Oceanogr., 4, 4, pp. 594-600.

Crombie, D. D., K. Hasselmann and W. Sell (1978). High-frequency radar observations of sea waves travelling in opposition to the wind. Bound. Layer Met., 13, 2, pp. 45-55.

Daley, J. C. (1973). Wind dependence of radar sea return. J. Geophys. Res., 78, 33, pp. 7823-7833.

De Rycke, R. J. (1973). Sea ice motions off Antarctica in the vicinity of the eastern Ross Sea as observed by satellites. J. Geophys. Res., 78, 36, pp. 8873-8879.

Diesen, B. C. III, and D. L. Reinke (1978). Soviet meteor satellite imagery. Bull A.M.S., 59, 7, pp. 804-807.

Dollar, R. A. and R. E. Cheney (1977). Observed formation of a Gulf Stream cold core ring. J. Phys. Oceanogr., 7, 6, pp. 944-946.

Douglas, B. C. and C. C. Goad (1978). The role of orbit determination in satellite altimeter data analysis. Bound. Layer Met., 13, pp. 245-253.

Downing, H. D. and D. Williams (1975). Optical constants of water in the infrared. J Geophys Res., 80, 12, pp. 1656-1661.

Dunne, J. A. (1978). The experimental oceanographic satellite SEASAT-A. Bound. Layer Met., 13, pp. 393-405.

Eittreim, S., E. M. Thorndike and L. Sullivan (1976). Turbidity distribution in the Atlantic Ocean. DSR, 23, pp. 1115-1127.

Elachi, C. (1976). Wave patterns across the North Atlantic on September 28, 1974 from airborne radar imagery. J. Geophys. Res., 81, 15, pp. 2655-2656.

Elachi, C. and J. R. Apel (1976). Internal wave observations made with an airborne synthetic aperture imaging radar. Geophys. Res. Ltrs., 3, 11, pp. 647-653.

Elachi, C. (1978). Radar imaging of the ocean surface. Bound. Layer Met., 13, pp. 165-181.

Estes, J. E. and L. W. Senger (1972). The multispectral concept as applied to marine oil spills. Remote Sens. of Envir., 2, pp. 141-165.

Fedor, L. S. and D. E. Barrick (1978). Measurement of ocean wave heights with a satellite radar altimeter. EOS Trans. AGU, 59, 9, pp. 843-847.

Fett, R. W. and K. M. Rabe (1976). Island barrier effects on sea state as revealed by a numerical model and DMSP satellite data. J. Phys. Oceanogr., 6, 3, pp. 324-344.

Flock, W. L. (1977). Monitoring open water and sea ice in the Bering Strait by radar. IEEE Trans. Geosci. Elect., GE-15, 4, pp. 196-202.

Forgan, B. W. (1977). Solar constants and radiometer scales. J Applied Optics, 16, pp. 1628-1632.

Fraser, R. S., Bahethi and A. H. Al-Abbas (1977). The effect of the atmosphere on the classification of satellite observations to identify surface features. Remote Sens of Envir., 6, pp. 229-251.

Galin, V. YA., M. S. Malkevich and L. M. Shukurova (1975). The transmission function in the 9.6 μm atmospheric ozone band. Atmos. Ocea. Phys., 11, 10, p. 640.

Gasparovic, R. F. and L. D. Tubbs. (19 ). Influence of reference source properties on ocean heat flux determination with two-wavelength radiometry. J. Geophys. Res., 80, 18, pp. 2667-2671.

Gavrilov, A. S. and D. L. Laykhtman (1973). Influence of radiative heat transfer on the conditions in the atmospheric surface layer. Atmos. Ocea. Phys., 9, 1, p. 12.

Gaynor, J. E., F. F. Hall, J. G. Edinger and G. R. Ochs (1977). Measurement of vorticity in the surface layer using an acoustic echo sounder array. Remote Sens of Envir., 6, pp. 127-139.

Georgiyevskiy, YU. S. et al. (1974). Effective transmission functions in the scattered light of the daytime sky. Atmos. Ocea. Phys., 10, 2, p. 92.

Gloersen, P. et al. (1974). Microwave mass of the polar ice of the earth. Bull. A.M.S., 55, 12, pp. 1442-1448.

Glossen, P. et al. (1973). Microwave signatures of first year and multi-year sea ice. J. Geophys Res., 78, 18, pp. 3564-3572.

Glushko, V. N. (1973). Polarization of the radiation of cloudless daytime sky in the 1.25-2.42 μm range. Atmos. Ocea. Phys., 9, 1, p. 48.

Gorchakov, G. I., A. A. Isakov and YU. S. Georgiyevskiy (1976). Correlations between the extinction coefficient and the directional light-scattering coefficients in the range of small angles. Atmos. Ocea. Phys., 12, 5, p. 311.

Golubitskiy, B. M. and M. V. Tantashev (1973). Properly conditioned use of the Monte Carlo method in solving certain optical transfer problems. Atmos. Ocea. Phys., 9, 11, p. 693.

Golubitskiy, B. M., I. M. Levin and M. B. Tantashev (1974). Brightness coefficient of a semi-infinite layer of sea water. Atmos. Ocea. Phys., 10, 11, p. 766.

Golubitskiy, B. M., N. V. Zadorina and M. V. Tantashev (1974). Cloud backscattering spectrum at 0.7-12 μm. Atmos. Ocea. Phys., 10, 1, p. 56.

Gordon, H. R. and O. B. Brown (1973). Irradiance reflectinity of a flat ocean as a function of its optical properties. Applied Optics, 12, pp. 1549-1551.

Gordon, H. R. and O. B. Brown (1975). Diffuse reflectance of the ocean: Some effects of vertical structure. Applied Optics, 14, pp. 2892-2895.

Gordon, H. R. and M. M. Jacobs (1977). Albedo of the ocean-atmospheric system, influence of sea foam. J. Applied Optics, 16, pp. 2257-2260.

Gordon, H. R. (1978). Removal of atmospheric effects from satellite imagery of the oceans. J. Applied Optics, 17, pp. 1631-1636.

Gordon, H. R. (1978). Remote sensing of optical properties in continuously stratified waters. J. Applied Optics, 17, pp. 1893-1897.

Greaves, J. R., P. E. Sherr and A. H. Glaser (1970). Cloud cover statistics and their use in the planning of remote sensing missions. Remote Sens. of Envir., 1, pp. 95-103.

Greenwood, J. A., A. Nathan, G. Neumann, W. J. Pierson, F. C. Jackson and T. E. Pease (1970). Radar altimetry from a spacecraft and its potential applications to geodesy. Remote Sens. of Envir., 1, pp. 59-71.

Greenwood, J. A., et al. (1970). Oceanographic applications of radar altimetry from a spacecraft. Remote Sens. of Envir., 1, pp. 71-81.

Grundlingh, M. L. (1974). A description of inshore current reversals off Richards Bay based on airborne radiation thermometry. DSR, 21, pp. 47-56.

Grundlingh, M. L. (1977). Drift observations from NIMBUS VI satellite tracked buoys in the southwestern Indian Ocean. DSR, 24, pp. 903-914.

Gurevich, I. YA and K. S. Shifrin (1976). Energetics of the lidar in remote detection of oil films on sea water. Atmos. Ocea. Phys., 12, 8, p. 527.

Hansen, D. V. and G. A. Maul (1970). A note on the use of sea surface temperature for observing ocean currents. Remote Sens. of Envir., 1, pp. 161-165.

Hans-Juergen, C. B., B. M. Kendall and J. C. Fedors (1978). Measurement of ocean temperature and salinity via microwave radiometry. Bound. Layer Met., 13, pp. 295-309.

Hanson, K. J. (1976). A new estimate of solar irradiance at the earth's surface on zonal and global scales. J. Geophys. Res., 81, 24, pp. 4435-4443.

Harger, R. O. and D. M. Levine (1978). Microwave scatter and sea state estimation: Two-scale ocean wave models. Bound. Layer Met., 13 pp. 107-119.

Harris, T. F. W., R. Legeckis and D. Van Foreest (1978). Satellite infra-red images in the Agulhas Current System. DSR, 25, pp. 543-548.

Hickman, G. D. and J. E. Hogg (1970). Application of an airborne pulsed laser for nearshore bathymetric measurements. Remote Sens. of Envir., 1, pp. 47-59.

Hojerslev, N. (1975). A spectral light absorption meter for measurements in the sea. LO, 20, 6, pp. 1024-1034.

Horvath, R., J. G. Braithwaite and F. C. Polcyn (1970). Effects of atmospheric path on airborne multispectral sensors. Remote Sens. of Envir., 1, pp. 203-217.

Huh, O. K. (1976). Detection of oceanic thermal fronts off Korea with the defense meteorological satellites. Remote Sens. of Envir., 5, pp. 191-215.

Ikeda, Y. and M. Stevenson (1978). Time series analysis of NOAA-4 sea surface temperature (SST) data. Remote Sens. of Envir., 7, pp. 349-363.

Ivanov, A. I., B. T. Tashenov and I. A. Fedulin (1975). Calculation of the daytime sky brightness in the visible and infrared regions of the spectrum. Atmos. Ocea. Phys., 11, 3, p. 189.

Ivanov, V. M. and YU. A. Savitskiy (1976). Certain possibilities for determination of underlying-surface temperatures from satellites in the 8-12 μm window. Atmos. Ocea. Phys., 12, 4, p. 261.

Jain, S. C. and J. R. Miller (1976). Subsurface water parameters: Optimization approach to their determination from remotely sensed water color data. J. Applied Optics, 15, pp. 886-890.

Jones, W. L. and L. C. Schroeder (1978). Radar backscatter from the ocean: Dependence on surface friction velocity. Bound. Layer Met., 13, pp. 133-151.

Johnson, W. R. and D. R. Norris (1977). A multispectral analysis of the interface between the Brazil and Falkland Currents from Skylab. Remote Sens. of Envir., 6, pp. 271-289.

Kadyshevich, YE. A., YU. S. Lyubovtseva and G. V. Rozenberg (1976). Light-scattering matrices of Pacific and Atlantic ocean waters. Atmos. Ocea. Phys., 12, 2, p. 106.

Kaiser, J. A. C. (1976). The use of pyranometers for underwater total radiant energy flux measurements. DSR, 23, pp. 881-887.

Kaiser, J. A. C. and R. H. Hill (1976). The influence of small cloud covers on the global irradiance at sea. J. Geophys. Res., 81, 3 pp. 395-398.

Kalmykov, A. I. and V. V. Pustovoytenko (1976). On polarization features of radio signals scattered from the sea surface at small grazing angles. J. Geophys. Res., 81, 12, pp. 1960-1964.

Kasevich, R. K. (1975). Directional wave spectra from daylight scattering. J. Geophys. Res., 80, 33, pp. 4535-4541.

Katsaros, K. B. and J. A. Businger (1973). Comments on the determination of the total heat flux from the sea with a two wavelength radiometer system as developed by McAlister. J. Geophys. Res., 78, 12, pp. 1964-1970.

Katsev, I. L. (1974). The reflection of a narrow light beam from a homogeneous isotropically scattering medium. Atmos. Ocea. Phys., 10, 4, p. 258.

Kattawar, G. W. and T. J. Humphreys (1976). Remote sensing of chlorophyll in an atmosphere-ocean environment: A theoretical study. J. Applied Optics, 15, pp. 273-282.

Ketchum, R. D. (1972). Airborne laser profiling of the Arctic pack ice. Remote Sens of Envir., 2, pp. 41-53.

Ketchum, R. D. and S. G. Tooma (1973). Analysis and interpretation of air-borne multifrequency side-looking radar sea ice imagery. J. Geophys. Res., 78, 3, pp. 520-538.

Kidder, S. Q. and T. H. Vonder Haar (1977). Seasonal oceanic precipitation frequencies from NIMBUS 5 microwave data. J. Geophys. Res., 82, 15, pp. 2083-2086.

Kirkham, R. B. and M. R. Stevenson (1976). Computer generated gridding of digital satellite imagery. Remote Sens. of Envir., 5, pp. 215-225.

Kirwan, A. D., G. McNally and J. Coehlo (1976). Gulf Stream kinematics inferred from a satellite tracked drifter. J. Phys, Oceanogr., 6, 5, pp. 750-755.

Klemas, V., J. F. Borchardt and W. M. Treasure (1972). Suspended sediment observations from ERTS-1. Remote Sens. of Envir., 2, pp. 205-223.

Klemas, V. and D. F. Polis (1977). A study of density fronts and their effects on coastal pollutants. Remote Sens. of Envir., 6, pp. 95-127.

Klemas, V., G. Davis, J. Lackie, W. Whelan and G. Tornatore (1977). Satellite, aircraft and drogue studies of coastal currents and pollutants. IEEE Trans. on Geosci. Elect., GE-15, 2, pp. 97-108.

Knowles, S. H. (1978). Oceanographic measurements using radio interferometer techniques. Remote Sens. of Envir., 7, pp. 339-349.

Kondrat'yev, K. Ya and O. I. Smoktin (1973). Influence of aerosols on the spectral albedo of the atmosphere-underlying surface system. Atmos. Ocea. Phys., 9, 12, p. 725.

Kopelevich, O. V. et al. (1975). A universal system of functions for approximation of the light-scattering phase functions of ocean water. Atmos. Ocea Phys., 11, 7, p. 486.

Kozlov, V. D. and N. M. Samson (1974). Measurement of the light attenuation factor in water from the backscattered light. Atmos. Ocea. Phys., 10, 10, p. 671.

Krasnokutskaya, L. D. and Ye. M. Feygel'son (1973). Calculation of infrared solar radiation fluxes in a cloudy atmosphere. Atmos. Ocea. Phys., 9, 10, p. 569.

Kretzberg, C. W. (1976). Interactive applications of satellite observations and mesoscale numerical models. Bull. A.M.S., 57, 6, pp. 679-685.

Kriebel, K. T. (1974). On the variability of the reflected radiation field due to differing distributions of the irradiation. Remote Sens. of Envir., 3, pp. 257-265.

Krishen, K. (1973). Detection of oil spills using a 13.3 G-Hz radar scatterometer. J. Geophys. Res., 78, 12, pp. 1952-1963.

Krishna Rao, P., A. E. Strong and R. Koffler (1971). Gulf Stream meanders and eddies as seen in satellite infrared imagery. J. Phys. Oceanogr., 1, 3, pp. 237-239.

Kropotkin, M. A. and T. YU. Sheveleva (1975). A study of the reflectance of ocean water and certain aqueous solutions at the wavelength 10.6 μm. Atmos. Ocea. Phys., 11, 2, p. 124.

Kunde, V. G. et al. (1974). The NIMBUS 4 infrared spectroscopy experiment 2, comparison of observed and theoretical radiances from 425-1450 $cm^{-1}$. J. Geophys. Res., 79, 6, pp. 777-784.

Kuo-Nan Liou (1976). On the absorption, reflection and transmission of solar radiation in cloudy atmospheres. JAS, 33, pp. 798-805.

Kurg, R. T. U. and J. Itzkan (1976). Absolute oil fluorescence conversion efficiency. J. Applied Optics, 15, pp. 409-415.

La Violette, P. E. (1974). A satellite aircraft thermal study of upwelled waters off Spanish Sahara. J. Phys. Oceanogr., 4, 4, pp. 685-689.

La Violette, P. E. and J. M. Hubertz (1975). Surface currents off the east coast of Greenland as deduced from satellite photographs of ice flows. Geophys. Res. Ltrs., 2, 9, pp. 400-402.

Legeckis, R. (1975). Application of synchronous meteorological satellite data to the study of the time dependent sea surface temperature change along the boundary of the Gulf Stream. Geophys. Res. Ltrs., 2, 10, pp. 435-438.

Legeckis, R. (1977). Oceanic polar front in the Drake Passage - satellite observations during 1976. DSR, 24, pp. 701-704.

Legeckis, R. (1978). A survey of worldwide sea surface temperature fronts detected by environmental satellites. J. Geophys. Res., 83, C9, pp. 4501-4522.

Lentz, R. R. (1974). A numerical study of electromagnetic scattering from ocean-like surfaces. Radio Science, 9, 12, pp. 1139-1146.

Leonard, D. A., B. Caputo, R. L. Johnson and F. E. Hoge (1977). Experimental remote sensing of subsurface temperature in natural ocean water. Geophys. Res. Ltrs., 4, 7, pp. 279-282.

Lerner, R. M. and J. P. Hollinger (1977). Analysis of 1.4 $GH_Z$ radiometric measurements from Skylab. Remote Sens. of Envir., 6, pp. 251-271.

Leslie, J. P. (1973). Exploratory study of the infrared characteristics of surface studies. Applied Optics, 12, pp. 2035-2036.

Levanov, N. (1971). Determination of sea surface slope distribution and wind velocity using sun glitter viewed from a synchronous satellite. J. Phys. Oceanogr., 1, 3, pp. 214-220.

Lipa, B. (1977). Derivation of directional ocean wave spectra by integral inversion of second order radar echoes. Radio Science, 12, 3, pp. 425-434.

Livshits, G. SH., V. L. Syachinov and E. L. Tem (1973). Determination of the optical thickness of the atmosphere from satellites. Atmos. Ocea. Phys., 9, 3, p. 169.

Lyons, W. A. and S. R. Pease (1973). Detection of particulate air pollution plumes from major point sources using ERS-1 imagery. Bull. A.M.S., 54, 11, pp. 1163-1170.

Lyzenga, D. R. (1978). Passive remote sensing techniques for mapping water depths and bottom features. J. Applied Optics, 17, pp. 379-383.

Malkevich, M. S. et al. (1973). The transparency of the atmosphere in the infrared. Atmos. Ocea. Phys., 9, 12, p. 718.

Maul, G. A. and D. V. Hansen (1972). An observation of the Gulf Stream surface front structure by ship, aircraft and satellite. Remote Sens. of Envir., 2, pp. 109-117.

Maul, G. A. and M. Sidran (1972). Comment on "Estimation of sea surface temperature from space." Remote Sens. of Envir., 2, pp. 165-171.

Maul, G. A. and M. Sidran (1973). Atmospheric effects of ocean surface temperature sensing from the NOAA satellite scanning radiometer. J. Geophys. Res., 78, 12, pp. 1909-1916.

Maul, G. A., R. L. Charnell and R. H. Qualset (1974). Computer enhancement of ERTS-1 images for ocean radiances. Remote Sens. of Envir., 3, pp. 237-255.

Maul, G. A., D. R. Norris and W. R. Johnson (1974). Satellite photography of eddies in the Gulf Loop Current. Geophys. Res. Ltrs., 1, 3, pp. 256-258.

Maul, G. A. and H. R. Gordon (1975). On the use of the earth resources technology satellite (LANDSAT-1) in optical oceanography. Remote Sens. of Envir., 4, 2.

Maul, G. A. (1978). Locating and interpreting hand-held photographs over the ocean; a Gulf of Mexico example from the Apollo-Soyuz test project. Remote Sens. of Envir., 7, pp. 249-265.

Maul, G. A., P. W. deWitt, A. Yanaway and S. R. Baig (1978). Geostationary satellite observations of Gulf Stream meanders: Infrared measurements and time series analysis. J. Geophys. Res., 83, C12, PP. 6123-6135.

Maykut, G. A. and T. C. Grenfell (1975). The spectral distribution of light beneath first-year sea ice in the Arctic Ocean. LO, 20, 4, pp. 554-563.

McCluney, W. R. (1976). Remote measurement of water color. Remote Sens. of Envir., 5, pp. 3-35.

McGrath, J. R. and F. M. Osborne (1973). Some problems associated with wind drag and infrared images of the sea surface. J. Phys. Oceanogr., 3, 3, pp. 318-327.

McNeill, D. and P. Hoekstra (1973). In-situ measurements on the conductivity and surface impedence of sea ice at VLF. Radio Science, 8, 1, pp. 23-30.

Memnger, R. P. (1977). Optical properties of turbid media with specularly reflecting boundaries: Applications to biological problems. J. Applied Optics, 16, pp. 2007-2012.

Miller, J. R., S. C. Jain, N. T. O'Neill, W. R. McNeil and K. P. B. Thomson (1977). Interpretation of airborne spectral reflectance measurements over Georgian Bay. Remote Sens. of Envir., 6, pp. 183-201.

Ming-Dah Chew (1974). An iterative scheme for determining sea surface temperatures, temperature profiles, and humidity profiles from satellite-measured infrared data. J. Geophys. Res., 79, 3, pp. 430-434.

Mitchell, O. R., E. J. Delp and P. L. Cheu (1977). Filtering to remove cloud cover in satellite imagery. IEEE Trans. Geosci. Elect., GE-15, 3, pp. 137-141.

Morel, A. and L. Brieur (1977). Analysis of variations in ocean color. LO, 22, 4, pp. 709-722.

Moskalenko, N. I. (1975). The effect of atmospheric aerosols on the spectral and angular distributions of thermal radiation. Atmos. Ocea. Phys., 11, 12, p. 785.

Mueller, J. L. (1976). Ocean color spectra measured off the Oregon coast: Characteristic vectors. J. Applied Optics, 15, 394-401.

Muench, R. D. and K. Ahlnas (1976). Ice movement and distribution in the Bering Sea from March to June 1974. J. Geophys. Res., 81, 24, pp. 4467-4481.

Murray, S. P., H. H. Roberts and W. J. Wiseman, Jr. (1975). An over-the-horizon radio direction finding system for tracking coastal and shelf currents. Geophys. Res. Ltrs., 2, 6, pp. 211-214.

Naumov, A. P. (1973). Interpretation of the atmosphere's radio emission in the 5 mm band. Atmos. Ocea. Phys., 9, 7, p. 394.

Nesmelova, L. I., S. D. Tvorogov and V. V. Fomin (1973). Calculation of the absorption coefficient of water vapor at 8-13 μm. Atmos. Ocea. Phys., 9, 11, p. 687.

Nesmelova, L. I. and S. D. Tvorogov (1973). The radiation coefficients of atmospheric gases. Atmos. Ocea. Phys., 9, 11, p. 690.

Neville, R. A. and J. F. R. Grower (1977). Passive remote sensing of phytoplankton via chlorophyll to fluorescence. J. Geophys. Res., 82, 24, p. 3487.

Nikitinskaya, N. I., O. D. Barteneva and L. K. Veselova (1973). Variations of the atmosphere's spectral (optical) aerosol thickness under conditions of high transparency. Atmos. Ocea. Phys., 9, 4, p. 242.

Noble, V. E. (1970). Ocean swell measurements from satellite photographs. Remote Sens. of Envir., 1, pp. 151-155.

Noble, V. E. and J. C. Wilkerson (1970). Sea surface temperature mapping flights, Norwegian Sea - summer 1968. Remote Sens. of Envir., 1, pp. 187-195.

Odell, A. P. and J. A. Wernman (1975). The effect of atmospheric haze on images of the earth's surface. J. Geophys. Res., 80, 36, pp. 5035-5040.

Orlov, A. P., V. V. Badayev, A. K. Gorodetskiy and M. S. Malkevich (1976). Aircraft studies of vertical infrared extinction profiles in the 10-12 μm window. Atmos. Ocea. Phys., 12, 7, p. 433.

Ostrom, B. (1974). Fertilization of the Baltic by nitrogen fixation in the blue-green algae. Remote Sens. of Envir., 3, pp. 305-311.

Otterman, J. (1974). Observations of wind streaklines over the Red Sea from the ERTS-1 imagery. Remote Sens. of Envir., 3, pp. 79-96.

Palm, C. S., R. C. Anderson and A. M. Reeca (1977). Laser probe for measuring 2-D wave slope spectra of ocean capillary waves. J. Applied Optics, 16, pp. 1074-1081.

Paltridge, G. W. (1974). Global cloud cover and earth surface temperature. JAS, 31, 6, pp. 1571-1576.

Paulson, C. A. and J. J. Simpson (1977). Irradiance measurements in the upper ocean. J. Phys. Oceanogr., 7, 6, pp. 952-956.

Pease, R. W. and L. W. Bowden (1970). Making color infrared film a more effective high-altitude remote sensor. Remote Sens. of Envir., 1, pp. 23-31.

Plant, W. J., W. C. Keller and J. W. Wright (1978). Modulation of coherent microwave backscatter by shoaling waves. J. Geophys. Res., 83, C3, pp. 1347-1352.

Plass, G. N., T. J. Humphreys and G. W. Rattamar (1978). Color of the ocean. J. Applied Optics, 17, pp. 1432-1446.

Platt, C. M. R. and A. J. Troup (1972). A direct comparison of satellite and aircraft infrared (10μm-12μm) remote measurements of surface temperature. Remote Sens. of Envir., 2, pp. 243-249.

Prishivalko, A. P. and Ye. K. Naumenko (1973). Optical back-scattering and extinction coefficients of aqueous aerosol. Atmos. Ocea. Phys. 9, 6, p. 372.

Prishivalko, A. P. and Ye. K. Naumenko (1974). Tables of extinction and backscattering coefficients for a water aerosol in the visible and near infrared. Atmos. Ocea. Phys., 10, 1, p. 52.

Probkakara, C., G. Dalu and V. G. Kunde (1974). Estimation of sea surface temperature from remote sensing in the 11 to 13 μm window region. J. Geophys. Res., 79, 33, pp. 5039-5044.

Probhakara, C. and G. Dalu (1976). Remote sensing of the surface emissivity at 9 μm over the globe. J. Geophys. Res., 81, 21, pp. 3719-3724.

Querry, M. R. et al. (1977) Relative reflectance and complex refractive index in the infrared from saline environmental waters. J. Geophys. Res., 82, 9, pp. 1425-1434.

Raschke, E., T. H. Vonder Haar, W. R. Bandeen and M. Pasternak (1973). The annual radiation balance of the earth-atmosphere system during 1969-1970 from NIMBUS 3 measurements. JAS, 30, 3, pp. 341-364.

Rayzer, V. YU., YE. A. Sharkov and V. S. Etkin (1975). Influence of temperature and salinity on the radio emission of a smooth ocean surface in the decimeter and meter bands. Atmos. Ocea Phys., 11, 6, p. 404.

Razumovskiy, I. T. (1973). Reducing the influence of sky radiation in radiation thermometer measurements of water surface temperatures. Atmos. Ocea Phys., 9, 12, p. 755.

Reed, R. K. and D. Halpern (1975). Insolation and net long wave radiation off the Oregon coast. J. Geophys. Res., 80, 6, p. 837.

Reed, R. K. (1975). Variations in oceanic net long wave radiation caused by atmospheric thermal structure. J. Geophys. Res., 80, 27, pp. 3819-3820.

Reed, R. K. (1976). On estimation of net long wave radiation from the oceans. J. Geophys. Res., 81, 33, pp. 5793-5794.

Richardsen, P. L., R. E. Cheney and L. A. Mantini (1977). Tracking a Gulf Stream ring with a free drifting buoy. J. Phys. Oceanogr., 7, 4, pp. 580-590.

Ross, D. B. and V. Cardine (1974). Observations of oceanic whitecaps and their relation to remote measurements of surface wind speed. J. Geophys. Res., 79, 3, pp. 444-452.

Ross, D. B. and W. L. Jones (1978). On the relationship of radar back-scatter to wind speed and fetch. Bound. Layer Met., 13, pp. 151-165.

Rouse, L. J. and J. M. Coleman (1976). Circulation observations in the Louisiana Bight using LANDSAT imagery. Remote Sens. of Envir., 5, pp. 55-67.

Rozenberg, V. I. and B. M. Vorob'yev (1975). Extinction of electromagnetic waves in the range 100 μm-17 cm in "warm" and supercooled clouds and fogs. Atmos. Ocea. Phys., 11, 5, p. 325.

Salomonson, V. V. and W. E. Marlatt (1972). Airborne measurements of reflected solar radiation. Remote Sens. of Envir., 2, pp. 1-9.

Savage, R. C. and J. A. Weinman (1975). Preliminary calculations of the upwelling radiance from rainclouds at 37.0 and 19.35 $GH_Z$. Bull. A.M.S., 56, 12, pp. 1272-1274.

Schroeder, W. W. (1977). Sea truth and environmental characterization studies of Mobile Bay, Alabama. Remote Sens. of Envir., 6, pp. 27-45.

Scully-Power, P. and P. Twitchell (1975). Satellite observation of cloud patterns over east Australian Current anticyclonic eddies. Geophys. Res. Ltrs., 2, 3, pp. 117.

Shemdin, O. H. et al. (1978). Comparison of in-situ and remotely sensed ocean waves off Marineland, Florida. Bound. Layer Met., 13, pp. 193-203.

Shenk, W. E. and V. V. Salomanson (1972). A multispectral technique to determine sea surface temperatures using NIMBUS 2 data. J. Phys. Oceanogr., 2, 2, pp. 157-167.

Sheu, P. J. and E. M. Agee (1977). Kinematic analysis and air-sea heat flux associated with mesoscale cellular convection during ANTEX 75. JAS, 34, 5, pp. 793-801.

Shifrin, K. S. (1974). Influence of wind on the effective radiation of the ocean. Atmos. Ocea. Phys., 10, 7, p. 495.

Shifrin, K. S. and M. M. Chernyak (1974). Thermal radiation of water droplets in the microwave region. Atmos. Ocea. Phys., 10, 10, p. 685.

Shifrin, K. S., O. V. Kopelevich, V. I. Burenkov and YU. L. Mashtakov (1974). Light scattering functions and structure of ocean hydrosols. Atmos. Ocea. Phys., 10, 1, p. 13.

Smerkalov, V. A. (1976). The optical mass of the real atmosphere as a function of wavelength. Atmos. Ocea. Phys., 12, 9, p. 609.

Smith, R. C. et al. (1973). Optical properties and color of Lake Tahoe and Crater Lake. LO, 18, 2, pp. 189-199.

Smith, R. C. and K. S. Baker (1978). The bio-optical state of ocean waters and remote sensing. LO, 23, 2 pp. 247-259.

Smith, R C. and K. S. Baker (1978). Optical classification of natural waters. LO, 23, 2, pp. 260-267.

Smith, W. L. and H. M. Woolf (1976). The use of Eigenvectors of statistical covariance matrices for interpreting satellite sounding radiometer observations. JAS, 33, pp. 1127-1140.

Snyder, R. L. (1973). On the estimation of the directional spectrum of surface gravity waves from a programmed aircraft altimeter. J. Geophys. Res., 78, 9, pp. 1475-1478.

Sobcyak, L. W. (1977). Ice movements in the Beaufort Sea, 1973-1975: Determination by ERTS imagery. J. Geophys. Res., 82, 9, pp. 1413-1418.

Sobti, A. and R. K. Moore (1976). Correlation between microwave scattering and emission from land and sea at 13.9 $GH_z$. IEEE Trans. Geosci. Elect., GE-14, 2, pp. 93-96.

Stavropoulos, C. C. and C. D. Duncan (1974). A satellite-tracked buoy in the Agulhas Current. J. Geophys. Res., 79, 18, pp. 2744-2746.

Stewart, R. H. and J. W. Joy (1974). HF radio measurements of surface currents. DSR, 21, pp. 1039-1049.

Stewart, R. H. and J. R. Barnum (1975). Radio measurements of oceanic winds at long ranges: An evaluation. Radio Science, 10, 10, pp. 853-858.

Stilwell, D. and R. O. Pilon (1974). Directional spectra of surface waves from photographs. J. Geophys. Res., 79, 9, pp. 1277-1284.

Strauch, R. B., W. C. Campbell, R. B. Chadwick and K. P. Moran (1975). Microwave FM-CW Doppler radar for boundary layer probing. Geophys. Res. Ltrs., p. 193.

Strong, A. E. (1974). Remote sensing of Algal blooms by aircraft and satellite in Lake Erie and Utah Lake. Remote Sens. of Envir., 3, pp. 99-109.

Strong, A. E. (1978). Chemical whitings and chlorophyll distributions in the Great Lakes as viewed by LANDSAT. Remote Sens. of Envir., 7, pp. 61-73.

Stumpf, H. G. and A. E. Strong (1974). ERTS-1 views an oil slick? Remote Sens. of Envir., 3, pp. 87-91.

Stumpf, H. G. (1975). Satellite detection of upwelling in the Gulf of Tehuantepec, Mexico. J. Phys. Oceanogr., 5, 2, pp. 383-388.

Stumpf, H. G. and P. K. Rao (1975). Evolution of Gulf Stream eddies as seen in satellite infrared imagery. J. Phys. Oceanogr., 5, 2, pp. 388-393.

Stumpf, H. G. and R. V. Legeckis (1977). Satellite observations of mesoscale eddy dynamics in the eastern tropical Pacific Ocean. J. Phys. Oceanogr., 7, 5, pp. 648-658.

Swift, C. T. (1974). Microwave radiometer measurements of the Cape Cod Canal. Radio Science, 9, 7, pp. 641-654.

Szekielda, K. H. and W. F. Mitchell (1972). Oceanographic applications of color-enhanced satellite imageries. Remote Sens. of Envir., 2, pp. 71-77.

Tashenov, B. T., E. L. Tem and I. A. Fedulin (1973). Determinations of the atmospheric-aerosol spectrum from the optical characteristics of the clear daytime sky. Atmos. Ocea. Phys., 9, 1, p. 171.

Taylor, S. E. and L. E. Williamson (1973). Satellite calibration site has brightness equivalent to clouds. Bull. A.M.S., 54, 6, p. 551.

Teague, C. C., G. L. Tyler, R. H. Stewart (1975). The radar cross section of the sea at 1.95 $MH_Z$: Comparison of in-situ and radar determinations. Radio Science, 10, 10, pp. 847-852.

Thekaekara, M. P. (1976). Solar irradiance: Total and spectral and its possible variations. J. Applied Optics, 15, pp. 915-921.

Theon, J. S. (1973). A multispectral view of the Gulf of Mexico from NIMBUS 5. Bull. A.M.S., 54, 9, pp. 934-937.

Thomann, G. C. (1976). Experimental results of the remote sensing of sea-surface salinity at 20-cm wavelength. IEEE Trans. Geosci. Elect., GE-14, 13, pp. 198-214.

Thomas, R. K. and H. N. Kritikos (1975). Measurement of sea state by RF interferometry. IEEE Trans. Geosci. Elect., GE-13, 2, pp. 73-80.

Timofeyev, N. A. (1975). Interpretation of radiation measurements on "meteor" satellites, and the basis for conversion from the albedo of the ocean-atmosphere system to the shortwave radiation at the ocean surface. Atmos. Ocea. Phys., 11, 1, p. 8.

Timofeyev, N. A. and YE. N. Shutova (1975). Angular structure of the upward longwave radiation field over the oceans. Atmos. Ocea. Phys., 11, 11, p. 850.

Tober, G., R. C. Anderson and O. H. Shemdin (1973). Laser instrument for detecting water ripple slopes. Applied Optics, 12, pp. 788-794.

Tomiyasu, K. (1974). A note on specular ocean surface radar cross section. J. Geophys. Res., 79, 21, p. 3101.

Tracton, M. S. and R. D. McPherson (1977). On the impact of radiometric sounding data upon operations numerical weather prediction at NMC. Bull. A.M.S., 58, 11, pp. 1201-1209.

Twomey, S. (1976). Computations of the absorption of solar radiation by clouds. JAS, 33, pp. 1087-1091.

Tyler, G. L., C. C. Teague, R. H. Stewart, A. M. Peterson, W. H. Munk and J. W. Joy (1974). Wave directional spectra from synthetic aperture observations of radio scatter. DSR, 21, pp. 989-1016.

Tyler, J. E. (1976). Ocean analysis by means of Beer's Law. J. Applied Optics, 15, pp. 2565-2567.

Valenzuela, G. R. (1978). Theories for the interaction of electromagnetic and oceanic waves - a review. Bound. Layer Met., 13, 2, pp. 61-87.

Van Melle, M. J., H. H. Wang and W. F. Hall (1973). Microwave radiometric observations of simulated sea surface conditions. J. Geophys. Res., 78, 6, pp. 969-976.

Viollier, M., P. Y. Deschamps and P. Lecomte (1978). Airborne remote sensing of chlorophyll content under cloudy sky as applied to the tropical waters in the Gulf of Guinea. Remote Sens. of Envir., 7, pp. 235-249.

Vonbun, F. O., J. G. Marsh and F. J. Lerch (1978). Computed and observed ocean topography: A comparison. Bound. Layer Met., 13, pp. 253-263.

Vukovich, F. M. (1974). The detection of nearshore eddy motion and wind-driven currents using NOAA 1 sea surface temperature data. J. Geophys. Res., 79, 6, pp. 853-860.

Vukovich, F. M. and B. W. Crissman (1974). Case study of exchange processes on the western boundary of the Gulf Stream using NOAA 2 satellite data and ship data. Remote Sens. of Envir., 3, pp. 169-171.

Vukovich, F. M. (1976). An investigation of a cold eddy on the eastern side of the Gulf Stream using NOAA 2 and NOAA 3 satellite data and ship data. J. Phys. Oceanogr., 6, 4, pp. 605-612.

Vukovich, F. M. and B. W. Crissman (1978). Observations of the intrusion of a narrow warm tongue into the Sargasso Sea using satellite and in situ data. J. Geophys. Res., 83, C4, pp. 1929-1934.

Wadhams, P. (1973). Attenuation of swell by sea ice. J. Geophys. Res., 78, 18, pp. 3552-3563.

Wadhams, P. (1975). Airborne laser profiling of swell in an open ice field. J. Geophys. Res., 80, 33, pp. 4520-4528.

Walsh, E. J. (1974). Analysis of experimental NRL radar altimeter data. Radio Science, 9, 9, pp. 711-722.

Walsh, E. J., E. A. Uliana and B. S. Yaplee (1978). Wave heights measured by a high resolution pulse-limited radar altimeter. Bound. Layer Met., 13, pp. 263-277.

Webster, W. J. et al. (1976). Spectral characteristics of the microwave emission from a wind driven foam covered sea. J. Geophys. Res., 81, 18, pp. 3095-3099.

Wendler, G. (1973). Sea ice observations by means of satellite. J. Geophys. Res., 78, 9, pp. 1427-1448.

Wentz, F. J. (1975). A two scale scattering model for foam-free sea microwave brightness temperatures. J. Geophys. Res., 80, 24, pp. 3441-3446.

Wentz, R. J. (1978). The forward scattering of microwave solar radiation from a water surface Radio Science, 13, 1, pp. 131-138.

Wetzel, Lewis B. (1977). A model of sea backscatter intermittancy at extreme grazing angles. Radio Science, 12, 5, pp. 749-756.

Wezernak, C. T. and D. R. Lyzenga (1974). Analysis of Cladophora distribution in Lake Ontario using remote sensing. Remote Sens. of Envir., 3, pp. 37-49.

Widger, W. K. and M. P. Woodall (1976). Integration of the planck blackbody radiation function. Bull. A.M.S., 57, 10, pp. 1217-1219.

Wilheit, T., W. Nordbergy, J. Blinn, W. Campbell and A. Edgerton (1972). Aircraft measurements of microwave emission from Arctic sea ice. Remote Sens. of Envir., 2, pp. 129-141.

Wilheit, T. (1978). A review of applications of microwave radiometry to oceanography. Bound. Layer Met., 13, pp. 277-295.

Wright, J. W. (1978). Detection of ocean waves by microwave radar; the modulation of short gravity-capillary waves. Bound. Layer Met., 13, 2, pp. 87-107.

Wrytki, K. (1977). Advection in the Peru Current as observed by satellite. J. Geophys. Res., 82, 27, pp. 3939-3944.

Yakubenko, V. G. et al. (1974). On the brightness fluctuations of an underwater light field. Atmos. Ocea. Phys., 10, 9, p. 621.

Yeske, L. A., T. Green, F. Scarpace and R. E. Terrell (1973). On current measurements in Lake Superior by photogrammetry. J. Phys. Oceanogr., 3, 1, pp. 165-167.

# 8. BOOK REFERENCES


Apel, J. R. (ed). Sea Surface Topography from Space. 2 vols., NOAA TR ERL 228-AOML 7, 1972.

Badgley, P. C. (ed). Oceans from Space. Symposium held in 1967. Gulf, 1969.

Barrett, E. & L. F. Curtis (ed). Environmental Remote Sensing. Bristol Symposium on Remote Sensing. Crane, Russak, 1974.

Chandrasenkhar, S. Radiative Transfer. Dover, 1960.

Cortright, E. M. Exploring space with a camera. NASA SP-168, U. S. Gov't Printing Off., 1968.

Cravat, H. R. & R. Glaser. Color Aerial Stereograms of Selected Coastal Areas of the United States . U. S. Gov't Printing Off., 1971.

Derr, V. E. (ed). Remote Sensing of the Troposhere. NOAA, U. S. Gov't Printing Off., 1972.

Duda, R. O. & P. E. Hart. Pattern Classification & Scene Analysis. Wiley, 1973.

Earth Photographs from Gemini III, & VI through XII. NASA SP-129, U. S. Gov't Printing Off., 1967.

Earth Photographs from Gemini VI through XII. NASA SP-171, U. S. Gov't Printing Off., 1968.

Estes, J. E. and L. W. Senger (eds). Remote Sensing; Technique for Environmental Analysis. Hamilton, 1973.

Ewing, G. C. (ed) Oceanography from Space. Woods Hole Oceanographic Inst., TR 65-10, 1965.

Gjessing, D. T. Remote Surveillance by Electromagnetic Waves. Ann Arbor Science Pubs., 1978.

Hecht, E. & A. Zajac. Optics. Addison-Wesley, 1974.

Handbook of Military Infrared Technology. Off. of Naval Research, 1965.

Henderson, S. T. Daylight and its spectrum. American Elsevier, 1970.

Hill, M. N. (ed). The Sea, Vol. 1. Interscience, 1966 (Ch.8 on light).

Holz, R. K. The Surveillant Science, Remote Sensing of the Environment. Houghton Mifflin, 1973.

Jenkins, A. & H. E. White. Fundamentals of Optics. McGraw-Hill, 1957.

Jensen, N. Optical and Photographic Reconnaissance Systems. Wiley, New York, 1968.

Jerlov, N. G. & E. S. Nielsen (eds). Optical Aspects of Oceanography. Symposium. Academic Press, 1972.

Jerlov, Nils G. Marine Optics. Elsevier, 1976.

Kondratyev, K. Ya. Radiation in the Atmosphere. Academic Press, 1969.

Kudritskii. D. M. Hydrographic interpretation of Aerial Photographs. Translated from Russian. Israel Program for Scientific Translations, 1966.

Lintz, J.& D. S. Simonett (eds). Remote Sensing of Environment, Addison-Wesley, 1976.

Long Maurice W. Radar Reflectivity of Land & Sea. Heath, 1975.

McCartney, E. J. Optics of the Atmosphere. Wiley, 1976.

Manual of Photogrammetry. American Society of Photogrammetry, 2 vols., 1966.

Manual of Remote Sensing. American Society of Photogrammetry, 2 vols., 1975.

Neblette, C. B. Fundamentals of Photography. Van Nostrand, 1970.

Nicks, Oran W., (ed). This Island Earth. NASA SP-250, U. S. Gov't Priniting Off., 1970.

Proc. of the International Symposium on Remote Sensing of the Environment. First through the Eleventh. Environ. Res. Instit. of Michigan, Ann Arbor, Michigan.

Remote Sensing. National Academy of Sciences, 1970.

Remote Sensing of Earth Resources and the Environment; seminar in depth. Proc., Soc. Photo-Optical Instrumentation Engrs., 1971.

Skolnik, M.I. Radar Handbook. McGraw-Hill, 1970.

SKYLAB Explores the Earth. NASA SP-380, U. S. Gov't Printing off., 1977.

Swain, P. H. and S. M. Davis (eds). Remote Sensing: The Quantitative Approach. McGraw-Hill, New York, 1978.

Symposium on Significant Results Obtained from the Earth Resources Technology Satellite-1. NASA SP-326, 2 vols., U. S. Gov't Printing Off., 1973.

Third Earth Resources Technology Satellite-1 Symposium. NASA SP-351, 2 vols., U. S. Gov't Printing Off., 1973.

Tyler, John E. Measurement of Spectral Irradiance Underwater. Gordon & Breach, 1970.

Univ. of Michigan Notes for a Program of Study in Remote Sensing of Earth Resources. 14 Feb. 1968 - 3 May 1968 conducted at NASA MSC, Houston, Texas. Univ. of Michigan, Willow Run Labs., Nov. 1968.

Valley, S. E. (ed). Handbook of Geophysics & Space Environment. U. S. Air Force Cambridge Resource Labs., 1965.

Verstappen, H. Th. Remote Sensing in Geomorphology. Elsevier, 1977.

Wenderoth , S. and E. Yost. Multispectral Photography for Earth Resources. Science Engr. Research Group, C. W. Post Univ., 1974.

Williams R. S. & W. D. Carter (eds). ERTS-1 A New Window on our Planet. Geological Survey Professional Paper 929, U. S. Gov't Printing Off., 1976.